Gut microbiota–mediated lipid accumulation as a driver of evolutionary adaptation to blue light toxicity in *Drosophila*

Yuta Takada[1], Toshiharu Ichinose[2,3], Naoyuki Fuse[4], Kokoro Saito[3], Wakako Ikeda-Ohtsubo[1], Hiromu Tanimoto[3], Masatoshi Hori[1]

[1]Graduate School of Agricultural Sciences, Tohoku University, Japan

[2]Frontier Research Institute for Interdisciplinary Sciences, Tohoku University, Japan

[3]Graduate School of Life Sciences, Tohoku University, Japan

[4]Graduate School of Pharmaceutical Sciences, Tohoku University, Japan

Correspondence to Yuta Takada or Masatoshi Hori

yutatakada38@gmail.com

masatoshi.hori.a3@tohoku.ac.jp

Abstract

Since the origin of life, the sunlight-driven environment on Earth has shaped the evolution of organisms. Blue light (BL), a major component of sunlight, is crucial to the biological processes of many insect species, yet excessive exposure can be highly toxic. BL toxicity can affect fitness and act as a selective pressure in insects. However, tolerance and evolutionary adaptation to this stressor remain largely unexplored. Here, we used *Drosophila melanogaster* as a model to select for BL tolerance over 60 generations. The selected line (SL) exhibited an obese phenotype accompanied by midgut elongation. Surprisingly, BL tolerance in the SL was dependent on gut microbiota–mediated lipid accumulation. In addition, we found that parental BL exposure plays a vital role in midgut elongation and increased abundance of beneficial bacteria. Whole-genome and transcriptome analyses consistently highlighted interactions between the microbiota and lipogenesis genes. Remarkably, manipulation of lipogenesis via these genes conferred BL tolerance even in the absence of selection. We hypothesise that the acquisition of BL tolerance occurs through 'adaptive obesity' by maximising the benefits of the gut microbiota. Our findings demonstrate that evolutionary adaptations to environmental stress can be driven by optimised interactions with the microbiota.

Introduction

Organisms utilize various environmental cues for survival, yet excessive exposure to these cues may make them stressors. Toxicity resulting from environmental stressors impacts the organisms' fitness and thus can drive their evolution.

Blue light (BL) is within the 400–500 nm range, is abundant in sunlight, and is crucial for insect physiology and ecology because it influences processes such as visual perception, circadian rhythms, and photoreactivation (Figure. 1)[1–4]. However, excessive BL exposure is lethal across various insect species, with toxicity varying by species and developmental stage[5,6]. We have demonstrated that exposure to BL at intensities below 40% of sunlight's BL content for several days can be lethal to fruit fly *Drosophila melanogaster* (hereinafter referred to as *Drosophila*), mosquito *Culex pipiens* form *molestus,* flour beetle *Tribolium confusum,* and leaf beetle *Galerucella grisescens*[5–7]. Notably, in *Drosophila*, *C. pipiens* f. *molestus*, and *G. grisescens*, BL around 420, 440, and 465 nm has been found to be more lethal than shorter wavelength 375–405 nm[5–7]. These results suggest that the sensitivity of BL toxicity cannot be explained by photon energy alone. In *Drosophila*, BL around 465 nm is particularly toxic to both pupae and adults, with males being more sensitive than females[5]. The BL toxicity is thought to be associated with reactive oxygen species (ROS) generated by mitochondria and other cellular components, leading to oxidative damage[5,8–12]. This damage can impair fitness and act as a selective pressure in insects, yet tolerance and evolutionary adaptation to this stressor remain largely unexplored.

Laboratory selection has contributed to understanding the evolutionary adaptations of organisms to environmental stressors[13,14]. *Drosophila* is well-suited for laboratory selection experiments due to its short life cycle and the extensive genetic and physiological knowledge available[15]. Importantly, these experiments often reveal both evolutionary responses and trade-offs that were not anticipated at the outset[16,17]. Here, by selecting flies that are tolerant to excessive BL exposure, we established *Drosophila* strain with enhanced BL tolerance. Characterization of these selected line (SL) flies revealed that obesity is a key

adaptive trait for enhanced BL tolerance. Surprisingly, we found that increased gut bacterial load is indispensable for the acquired BL tolerance. This study highlights that optimized interaction with the gut microbiota was the key for evolutionary adaptation in the host.

Results

Drosophila evolved BL tolerance through laboratory selection

We first generated a *Drosophila* strain with BL tolerance through laboratory selection (Figure. 2A). Over the generations, 1–5 day-old flies were exposed for 3 days to BL at around 465 nm, a wavelength highly toxic to *Drosophila* adults, at a photon flux density at which approximately 50% of individuals exhibited the “low impact” phenotype, which was defined as being capable of climbing after a 2-day recovery (Figure. S1A). We then selected the low impact flies and let them breed to develop the SL lines. The unselected control line (UCL), maintained without BL irradiation, served as a negative control for comparative analyses with the SL. In the negative control group, BL irradiation was replaced with darkness, and UCL parents were chosen randomly. Although not selected, a subset of UCL flies in each generation was exposed to BL under the same conditions as the SL to serve as a positive control group (Figure. S2A). This procedure was replicated in three independent lines for each group and each line was repeated for over 60 generations.

BL irradiation decreased the fecundity of the UCL flies by inhibiting ovarian development (Figure. 2B, C). However, the SL flies started to show improved adaptability after around 20 generations of selection, when despite continued BL irradiation, fecundity and ovarian development were maintained at similar levels to those of flies in the UCL (negative control group) (Figure. 2D–F and Figure. S1B and Data S1). Ovarian development was affected little by BL exposure in the SL flies but severely in the UCL flies (Figure 2E, F and Data S1). Moreover, fecundity in SL flies was slightly increased in response to BL irradiation, whereas that in UCL flies was reduced (Figure. 2G and Data S1). Additionally, SL flies survived longer than UCL flies under continuous BL irradiation (Figure. 2H and Data S1). These results

collectively suggest that we have successfully established a new *Drosophila* strain with enhanced BL tolerance.

SL flies exhibited obese phenotype, lipid accumulation, and oxidative stress resistance

Next, we examined the phenotypic characteristics of the SL flies. We noticed that they exhibited an obese phenotype characterized by abdomen bloating, increased body weight, and well-developed fat bodies with markedly increased lipid droplets (Figure. 3A–D and Data S2). They also showed an elongated midgut and shortened wings (Figure. 3E and Figure. S2A, B and Data S2). Additionally, we observed a slightly low number of oocytes in the SL flies (Figure. S2C and Data S2) and a strong inter-individual correlation between oocyte number and body weight in the UCL flies (Figure S2D and Data S2). SL flies maintained higher body weight than UCL flies despite similar food consumption levels (Figure. 3F and Data S2). Taken together, these results show that the increased body weight of SL flies was not due to larger ovaries or higher food intake but may instead be associated with increased lipid reserves and elongated midguts. SL flies were rich in major lipids, including fatty acids (fatty acid methyl esters, FAME) and triacylglycerol (TAG), and were starvation resistant, providing evidence of lipid accumulation (Figure. 3G–I and Data S2). Consistent with previous reports that lipid droplets and their constituent TAG may protect against oxidative damage[18–20], resistance to oxidative stress was higher in SL flies than in UCL flies (Figure. 3J and Data S2).

We did not find any physical traits associated with light reflection by cellular melanin, despite previous reports suggesting these as adaptive traits to phototoxicity (Figure. S2E)[21].

Increased bacterial abundance in SL flies

Gut microbiota–derived acetate serves as a substrate for de novo lipogenesis in the host through acetyl-CoA[22-25]. Considering the elongated midgut and accumulated lipids in SL

flies, we compared the gut microbiota profiles and amounts in SL and UCL flies. In both lines, 16S rRNA gene sequencing of whole-body DNA revealed that a single species of *Acetobacter* (*A. persici)*, a common gut bacteria in *Drosophila*, dominated (>99%) the microbiota (Figure. S3A and Data S3)[26]. Notably, bacterial counts were higher in SL flies than in UCL flies, and a positive correlation was observed between body weight and bacterial abundance, without any change in the microbiota profiles (Figure. 4A and Figure. S3B, C and Data S3). All randomly sequenced colonies were identified as *A. persici* (Data S3).

Gut microbiota promotes BL tolerance and lipid accumulation in SL flies

Following BL irradiation, both bacterial abundance and body weight in SL flies drastically decreased (Figure. 4B, C), suggesting that sensitivity of these flies to BL toxicity might be related to gut microbiota. Additionally, acetic acid bacteria, including *Acetobacter*, are known to influence fecundity and TAG levels in *Drosophila*[23,27–34]. To test the hypothesis that gut microbiota play a role in shaping the phenotype of SL flies, we used an antibiotic mixture (Abx) that depletes the bacterial abundance (Figure. S4A). Interestingly, we found that BL tolerance in the SL flies, as measured by fecundity, was totally abolished by Abx treatment, suggesting the critical role of gut microbiota (Figure. 4D and Data S3). Feeding the Abx-treated SL flies with the gut contents of SL flies rescued these phenotypes, whereas feeding with those of UCL flies barely did (Figure. S4B–D and Figure. 4D and Data S4). Consistently, Abx treatment significantly reduced the body weight and the TAG level selectively in the SL flies (Figure. 4E, F and Data S3). This result highlights the dependence of SL flies' body weight and lipid accumulation on their gut microbiota.

The midgut of Abx-treated SL flies was longer than that of UCL flies regardless of treatment, and it was even longer in non-treated SL flies (Figure. 4G and Data S5). A positive correlation between body weight and midgut length in non-treated SL flies (Figure. S5A and Data S5) suggested that gut microbiota may contribute to midgut elongation. Furthermore,

enhanced oxidative stress resistance was observed only in non-treated SL flies (Figure. S5B, C and Data S5). These observations align with previous reports that gut microbiota is linked to gut morphology and oxidative stress resistance[26,35,36]. Overall, these results suggest that the characteristic phenotype in SL flies is shaped by their gut microbiota.

Host genome and transcriptomic profiles explain the characteristic phenotype of SL flies

To investigate how the SL flies develop their phenotypes through interactions with gut microbiota, we conducted whole-genome sequencing to detect common variants selected in SL flies. Homozygous variants shared among the three replicate lines in SL and absent in UCL and in the wild type (Canton-S strain) were identified. SL-specific SNPs and indels were detected in 633 and 1936 genes, respectively, giving a total of 2224 genes, and the majority of alterations were located outside the coding sequences (CDS) (Figure. 5A and Data S6). Enrichment analysis using the Kyoto Encyclopedia of Genes and Genomes (KEGG) identified the Hippo signaling pathway as the only significantly enriched pathway (Figure. 5B), consistent with its known function in intestinal elongation[37,38]. Especially, the presence among the CDS variants of genes regulated by the Hippo signaling pathway (*Par-1*, *Misshapen*)[38–40], together with the elongated midgut observed in Abx-treated SL flies, suggests that midgut elongation in SL flies was potentially influenced by these variants (Data S6 and Figure. 4G).

Because mutations located outside the CDS are generally thought to influence gene expression and because gut microbiota may alter host phenotypes through changes in the host transcriptome[41], we performed transcriptome analysis on the whole body of non-irradiated UCL and SL flies, with or without the Abx treatment. We identified 1242 differentially expressed genes (DEGs), of which 1192 (96%) were specific to non-treated SL flies (Figure. 5C and Data S6). KEGG analysis of the 1192 DEGs revealed gene enrichment in oxidative phosphorylation, metabolic pathways, Toll and Imd signaling, and the TCA cycle

(Figure. 5D and Data S6). Suppressed mitochondrial metabolism is known to lead to lipid accumulation in various animal species[42,43]. Consistent with this fact, non-treated SL flies showed downregulation of most of the genes involved in oxidative phosphorylation and the TCA cycle, which are associated with mitochondrial metabolism (Figure. 5E). In addition, several genes whose downregulation is known to induce lipid accumulation were also specifically downregulated in non-treated SL flies (Figure. 5E)[44–46], including *Tachykinin* (*Tk*), which also harbored mutations in the SL flies (Figure. 5E and Data S6). Actually, *Tk* expression is known to be modulated in response to acetate produced by gut microbiota, thereby regulating lipid utilization in enterocytes[23,47]. Our results suggest that the phenotypes of SL flies are influenced by the Hippo signaling pathway, *Tk*, and mitochondrial genes, and by their interactions with gut microbiota.

Lipid accumulation via genetic manipulation confers BL tolerance

To prove the causal relationship between lipid accumulation and BL tolerance, we examined BL tolerance in genetically manipulated flies that are reported to have increased TAG levels[41,42]. We used a range of mutants and GAL4/UAS-mediated manipulations, including knockdowns of *Tk*, *Adipokinetic hormone receptor* (*AkhR*), and *Lipid storage droplet-1 (Lsd-1*), which were downregulated in the SL flies (Figure. 5E and Data S6 and Data S7). Interestingly, knocking down these genes enhanced BL tolerance to a level comparable to that in the SL flies (Figure. 6A). Furthermore, BL tolerance was also enhanced by other genetic manipulations that are known to increase lipid levels but were not detected as DEGs in our transcriptome analysis (Figure. 5E), such as knockdown of *brummer* (*bmm*), *Phosphatase and tensin homolog* (*Pten*), and *Stromal interaction molecule* (*Stim*), and overexpression of *Insulin-like receptor* (*InR*), *Lk6 kinase* (*Lk6*), and *Lipid storage droplet-2* (*Lsd-2*) (Figure. 6A). Indeed, we found a significant positive relationship between fecundity and TAG levels among flies with all of these genetic modifications (Figure. 6B), which strongly suggests that lipid accumulation is a trait that confers BL tolerance.

Parental BL irradiation affects progeny's gut microbiota–associated traits

Finally, we investigated why only the gut contents from SL flies could rescue BL tolerance in infection experiments, despite the dominance of the same gut bacterial species across strains (Figure. S3A and Figure. 4D). We noticed that the flies used for gut contents had different parental experiences depending on whether they belonged to the UCL or SL. Thus, we hypothesized that parental exposure to BL irradiation might influence gut microbiota–associated traits in the progeny, leading to quantitative or qualitative changes in gut microbiota. We examined the body weight and BL tolerance in Abx-treated SL flies that were fed with gut contents from flies whose parents had or had not received BL irradiation. Abx-treated SL flies fed with gut contents from SL flies whose parents had experienced BL irradiation showed the greatest increase in body weight (Figure. S6A and Data S8). However, flies fed with gut contents from *A. persici* in different cocktails, each standardized in concentration, exhibited similar body weight increases (Figure. S6B and Data S8). This suggests that quantitative rather than qualitative changes in gut microbiota due to parental BL irradiation are responsible for the increases in host body weight. Furthermore, gut contents from UCL flies whose parents had experienced BL irradiation also rescued the phenotypes of Abx-treated SL flies, restoring fecundity to the level conferred by gut contents from SL flies (Figure. 7A and Data S8 and Data S9). These results indicate that parental BL irradiation affects the progeny's bacterial abundance. Consistent with this idea, parental BL irradiation increased the progeny's body weight, bacterial abundance, and midgut length in both UCL and SL flies (Figure. S7 and Figure. 7B, C and Data S10). Notably, even without parental BL irradiation, the midgut of SL flies was longer than that of non-irradiated UCL flies, suggesting that this inherited trait had been conserved during the laboratory selection of SL flies (Figure. 7C). In both strains, parental BL irradiation induced midgut elongation even after antibiotic treatment, suggesting that in *Drosophila* this is a common response dependent on parental experience.

Discussion

In this study, we established BL-tolerant *Drosophila* strains through laboratory selection, demonstrating that excessive BL irradiation drives the 'adaptive obesity', particularly lipid accumulation mediated by gut microbiota. This supports the increasingly recognized role of microbiota in host adaptation to environmental stress, in which specific bacterial populations contribute to adaptive host phenotypes[32,48–51]. Our findings further reveal that elongation of the host midgut in response to parental BL toxicity facilitates an increase in beneficial bacteria, ultimately enhancing host fitness via lipid accumulation under excessive BL exposure (Figure. 8). This is the first description of the adaptation mechanisms of insects against BL toxicity.

SL flies exhibited increased lipid accumulation (Figure. 3), and genetic manipulation that increased lipid contents conferred BL tolerance (Figure. 6). This acquisition of BL tolerance can be explained by the role of lipid accumulation in protecting against ROS, which are produced upon BL irradiation[10,11]. Intracellular lipid droplets play a critical role in shielding cells from oxidative stress, as reduced TAG levels are associated with increased sensitivity to such stress[18–20,52]. Indeed, the accumulation of lipid droplets in response to intracellular ROS has been observed in many species[20,52]. Additionally, lipid droplets are closely linked to fecundity, as higher TAG levels are associated with improved fecundity, whereas reduced TAG levels can lead to oocyte degeneration[53,54]. Thus, lipid accumulation not only helps defend against BL toxicity but also supports the maintenance of fecundity. Furthermore, the transcriptome of SL flies revealed a broad downregulation of genes for mitochondrial metabolism (Figure. 5E). Mitochondria, while crucial for energy production, also contribute to ROS generation[55]. Therefore, the inhibition of both mitochondrial metabolism and lipid utilization could be an adaptive strategy to accumulate lipids while minimizing oxidative stress.

We identified *A. persici* as the predominant bacterial species and showed the critical role of its increased abundance in the acquisition of BL tolerance. *Acetobacter* species, which are well-known symbionts of *Drosophila* and other insects, are recognized for their acetate production[56]. Acetyl-CoA, derived from acetate, is essential for lipid utilization[25,57] and also plays a crucial role in the acetylation of both histone and non-histone proteins, facilitating adaptive responses through tissue plasticity[23,58,59]. The elevated TAG levels observed in SL flies may be explained by the increased acetyl-CoA pool resulting from gut microbiota–derived acetate. Additionally, gut microbiota might act as a barrier against physiological stress induced by BL toxicity. The significant reduction in gut microbiota following BL irradiation in SL flies (Figure. 4B) suggests the evolution of mechanisms that utilize bacteria as a direct nutritional resource. These findings align with previous research showing that *Acetobacter* enhances the fecundity and oxidative stress resistance of the host fly[26,32–34].

The increase in bacterial abundance appears to be associated with midgut elongation and genetic changes, particularly those in the Hippo signaling pathway (Figure. 4G and Figure. 5B). We also found that parental irradiation with BL, when combined with accumulated mutations in later generations of SL flies, is critical for the midgut elongation and bacterial abundance (Figure. 7B, C). This is consistent with previous studies showing that parental exposure to environmental stressors, such as starvation, induces epigenetic inheritance or alternations in the transcriptome[60,61]. In *Drosophila*, the midgut undergoes plastic elongation or shortening in response to environmental conditions[62,63]. This physical expansion of the gut, which increases spatial capacity, offers several advantages, including more efficient nutrient absorption, increased bacterial abundance, and maintenance of gut homeostasis[53,64–68]. However, midgut elongation alone, even after one generation with parental exposure to BL toxicity, is insufficient for BL tolerance (Figure. 2D and Figure. 7C). Full BL tolerance requires both midgut enlargement and specific genetic changes. Among these genetic factors, the genes for the neuropeptide *Tk* and its receptor *TkR99D* are

particularly important (Figure. 6 and Data S6), as they may regulate lipid utilization in response to acetate produced by the gut microbiota[23,46].

In conclusion, our findings underscore the importance of gut microbiota–mediated lipid accumulation as an adaptive trait for BL tolerance. The elongation of the midgut, associated with an increased abundance of beneficial bacteria, turns out to be a key factor in this evolutionary adaptation. Such phenotypes may be driven by genetic and epigenetic changes from selective pressures and parental BL exposure. These evolutionary responses to excessive BL exposure demonstrate how host traits evolve under a toxic BL environment by maximizing the benefits provided by gut microbiota. Our findings demonstrate that evolutionary adaptations to environmental stress can be driven by optimized interactions with microbiota.

Methods

Fly cultures and diet

Flies were maintained at 23–26°C on a 16:8 hour light:dark cycle using cold cathode fluorescent lamps as the light source. Detailed lighting conditions are provided in Data S1. The fly diet consisted of 5 g glucose (Fujifilm Wako Pure Chemicals Co., Osaka, Japan), 6 g dry brewer's yeast (Asahi Group Holdings Ltd., Tokyo, Japan), 1 g agar (Fujifilm Wako Pure Chemicals Co.), 0.4 mL propionic acid (Fujifilm Wako Pure Chemicals Co.), 0.4 mL 70% ethanol (Fujifilm Wako Pure Chemicals Co.), 0.01 g butyl *p*-hydroxybenzoate (Fujifilm Wako Pure Chemicals Co.), and 100 mL distilled water.

BL irradiation

Virgin flies aged 1–5 days were used. Unless otherwise specified, flies were exposed to 462 nm BL for 3 days. BL irradiation conditions varied across experiments:

Figure. 2C–G, 4D, 7A–C: Photon flux density 10.3×10^{1} photons·m^{-2}·s^{-1} for females.

Figure. 2C–G, Figure. 7B and C: 6.5×10^{1} photons·m^{-2}·s^{-1} for males.

Figure. 2H: 8×10^{1} photons·m^{-2}·s^{-1} for males and 10×10^{1} photons·m^{-2}·s^{-1} for females.

Figure. 6: 465 nm BL, 9.5×10^{1} photons·m^{-2}·s^{-1} for females.

For details see Data S1.

Irradiation was performed in a multi-room incubator (LH-30CCFL-8CT; Nippon Medical & Chemical Instruments Co., Ltd, Osaka, Japan) at 24–26°C, with LED panels (IS-mini®, ISL-150 × 150 Series; CCS Inc., Kyoto, Japan) installed on the ceiling. Photon flux density was measured using a high-resolution spectrometer HSU-100S (Asahi Spectra Co., Ltd., Tokyo, Japan) with ND 0050 filter (Asahi Spectra Co., Ltd) and spectroradiometer MS-730 (EKO Instruments Co., Ltd., Tokyo, Japan).

Laboratory selection for BL tolerance

Artificial selection

We used the Canton-S strain of *Drosophila*, a common wild-type strain, as the ancestral population for laboratory selection. Two strains were established, SL and UCL; the former was subjected to BL toxicity every generation and the latter was used for controls. Each strain included three replicate lines. For each strain, 60–100 virgin flies aged 1–5 days were placed in two 60 mm × 90 mm glass Petri dishes for BL irradiation. SL and UCL flies (positive control group) were exposed to 462 nm BL for 3 days. Instead of BL irradiation, the UCL, used as a negative control group, was kept in darkness for 3 days.

Climbing assay

Irradiated flies were placed in a breeding environment (for details, see “Fly cultures and diet” in Methods) for a 2-day recovery period. For the data shown in Figure. S1A and Figure. S4C, the impact of BL toxicity was assessed in a 4-minute climbing assay and the flies were categorized into five states:

“Low impact” (capable of climbing):

1. Intact: climbing >2 cm (This state is defined from the 17th generation)
2. Semi-intact: capable of climbing, but less efficiently

“High impact” (unable to climb):

3. Phase 1: alive but unable to climb
4. Phase 2: alive but non-ambulatory
5. Phase 3: dead

Artificial selective breeding and evaluation of fecundity

"Low impact" SL flies were allowed 5 days for mating and egg-laying. Each vial containing 3 mL of diet medium 3-mL contained 9–13 pairs, with a total of 4–8 vials (for details, see Data S1). After 5 days, the diet medium containing eggs and larvae was transferred to a larger plastic box (40 mL diet medium, 72 × 72 × 100 mm; Insect Breeding Square Dish, SPL Life Sciences, Gyeonggi-do, Korea) to ensure sufficient food supply. One box was used for

every 4 or 5 vials. UCL parents were randomly chosen from the negative control group (for details, see "Laboratory selection for BL tolerance -Artificial selection-" in Methods) and reared under the same conditions as the SL flies. The total number of pupae was counted and divided by the number of parents to determine the fecundity per female for each generation.

Survival assays

Virgin flies aged 5–10 days were used. In the continuous BL irradiation assay, 50 or 42 flies were placed in each glass Petri dish containing standard diet medium and exposed to 462 nm BL for 120 h. In the starvation assay, 10 flies were placed in each vial with 1% (w/v) agar (Fujifilm Wako Pure Chemicals Co.) in distilled water. In the oxidative stress assay, 10 flies were placed in each vial with a medium prepared with either 10 mM paraquat dichloride standard (Fujifilm Wako Pure Chemicals Co.) (Figure. 3I) or 10 mM 1,1'-dimethyl-4,4'-bipyridinium dichloride (Tokyo Chemical Industry Co., Ltd., Tokyo, Japan) (Figure. S5B and C), 5% (w/v) glucose (Fujifilm Wako Pure Chemicals Co.), and 1% (w/v) agar (Fujifilm Wako Pure Chemicals Co.) in distilled water. The surviving flies were manually counted every 2 h.

Measurement of fecundity

To measure fecundity (Figure. 2G, Figure. 4D, Figure. 6, and Figure. 7A), after 3 days of darkness (non-irradiation) or BL irradiation followed by a 3-day recovery period, 5 surviving females were randomly chosen and mated with 5 non-irradiated virgin males (aged 1–10 days) in individual pairs within vials containing 5 mL of diet medium for 4 days of egg-laying. The total numbers of pupae and emerged adults were counted to evaluate fecundity and emergence rate (in Figure. 2G, only the total number of pupae was measured).

Figure. 3G used non-irradiated males from the UCL or SL, Figure. 6 used non-irradiated Canton-S males, and Figure. 4D and Figure. 7A used non-irradiated Abx-treated males from the UCL or SL.

Measurement of body weight, organ size and oocyte number

Virgin flies aged 4–12 days were anesthetized by chilling on ice. Body weight was measured using an AUW220D balance (Shimadzu, Kyoto, Japan).

Wings or ovaries were dissected and photographed under a SteREO Discovery.V12 stereomicroscope and an Axiocam 305 color camera (Carl Zeiss, Oberkochen, Germany). Wing length was measured as the distance between the alula opening and the distal edge of the 3rd longitudinal vein, using Fiji ImageJ2 (version 2.3/1.54f), following a previous method[69]. Stage 14 oocytes were counted under the stereomicroscope. Midgut lengths of regions R1 to R5 were measured manually from the midgut images using Fiji ImageJ2[68].

Lipid droplet staining and imaging

We performed dissection and fluorescence microscopy to visualize lipid droplets in the fat body of the abdominal epithelium from virgin female flies aged 6–12 days. After removing other tissues from the abdomen, we fixed the abdominal epithelium in PBS containing 4% paraformaldehyde (Fujifilm Wako Pure Chemicals Co.) for 20 minutes. After fixation, we washed the samples twice with PBS (Gibco, Carlsbad, CA, USA) for 15 minutes each time. The fixed abdominal epithelium was stained with Nile Red (Fujifilm Wako Pure Chemicals Co.) at a concentration of 10 μg/mL overnight according to a previous method[70]. Following this, we washed the samples twice with PBS for 10 minutes each time and then stained them with NucBlue (Thermo Fisher Scientific, Waltham, MA, USA) for 3 minutes, followed by a 5-minute wash with PBS. All staining procedures were conducted in a light-shielded environment at room temperature. Imaging was performed under an Eclipse Ti2 microscope equipped with a DS-Ri2 camera (Nikon, Tokyo, Japan). The images were analyzed using

the Python package OpenCV (Python version 3.8.3 version 4.5.3.56) to obtain the mean fluorescent intensity of Nile Red.

Lipid extraction and derivatization of fatty acids

Lipids were extracted using the Bligh and Dyer method[71,72]. We homogenized 2 virgin female flies aged 6–12 days in 100 μL of PBS (Gibco), added 600 μL of methanol (Fujifilm Wako Pure Chemicals Co.) and chloroform (Fujifilm Wako Pure Chemicals Co.) in a 2:1 (v/v) ratio, vortexed for 1 minute, and shaken at 1000 rpm at 4°C for 2 h. Next, we added 200 μL of chloroform and 250 μL of distilled water, vortexed for 1 min, centrifuged at 9000 rpm for 2 min, and collected the organic lower phase. We then added 400 μL of chloroform to the remaining mixture, vortexed for 1 minute, and centrifuged as above. The two organic extracts were pooled and dried under vacuum. The dried lipids were derivatized using the Fatty Acid Methylation Kit (Nacalai Tesque, Inc., Tokyo, Japan) and the Fatty Acid Methyl Ester Purification Kit (Nacalai Tesque, Inc.). FAMEs were collected.

Gas chromatography mass spectrometry (GC-MS) analysis

The FAMEs were analyzed using a GC-MS instrument (GCMS-QP2010 Ultra (Shimadzu)) equipped with a DB-5 ms column (30 m × 0.25 mm ID, 0.25 μm film thickness) (J&W Scientific, Folsom, CA, USA). Helium was used as the carrier gas at a pressure of 100 kPa. The column oven was set at 40°C for 5 minutes. The temperature was increased at a rate of 10°C/min to 280°C and maintained at 280°C for 10 minutes. The injection port temperature was 220°C, and the analysis was performed in split mode. Fatty acids were identified using a similarity search against the standards Supelco F.A.M.E. Mix C4-C24 (Supelco, Bellafonte, PA, USA) and relevant references[73,74]. The total ion chromatogram area for each compound was measured. On the basis of the obtained data, we compared the total amount of FAMEs. The log-transformed average values of each compound in each replicate line were

visualized using a cluster map. Clusters were classified by hierarchical clustering using the Ward method based on Euclidean distances between compound amounts[75].

Measurement of TAG

Relative TAG levels were measured by homogenizing 10 virgin female flies (aged 6–12 days) in 1 mL of PBS (Fujifilm Wako Pure Chemicals Co.) containing 0.1% Triton X-100 (Nacalai Tesque Inc.). The homogenate was heated at 70°C for 10 minutes and then centrifuged at 20,000 × *g* for 15 minutes at 4°C. A 10-μL aliquot of the supernatant was used for TAG measurement using the LabAssay Triglyceride kit (Fujifilm Wako Pure Chemicals Co.). For protein normalization, protein concentration was measured using the Bradford method with the Protein Assay CBB Clean Up Kit and Protein Assay CBB Solution (both from Nacalai Tesque Inc.), with the standard calibration curve prepared using bovine serum albumin solution (Nacalai Tesque Inc.). Absorbance was measured using the BioTek Synergy H1 Multimode Reader (Agilent Technologies Inc., Santa Clara, CA, USA). Relative TAG levels were normalized to protein content, adjusted on the basis of the average values from UCL (Figure. 3G and Figure. 6) or non-treated UCL (Figure. 4F), and the Log_2 fold change was computed accordingly.

Measurement of reflectance and transmittance

Virgin female flies aged 6–12 days were anesthetized on ice. The abdominal reflectance and transmittance were measured by capturing hyperspectral images under a BX51WI microscope (Olympus, Tokyo, Japan) fitted with an SC-108 hyperspectral imaging system (EBA Japan Co., Ltd., Tokyo, Japan).

DNA extraction

Virgin female flies aged 5–8 days were used. For Figure. 5A and Figure. S3A, the same sample of 30 flies was used, with 10 flies used specifically for Figure. S3C. The flies were

rinsed in a 1.5-mL tube with 99% ethanol (Fujifilm Wako Pure Chemicals Co.) for 30 seconds. Then, 180 µL of PBS and beads were added, and the flies were homogenized at 3500 rpm for 30 seconds using the Micro Smash MS100R (Tomy Seiko Co., Ltd., Tokyo, Japan) while keeping the mixture cold. DNA was extracted using the DNeasy Blood & Tissue Kit (Qiagen, Hilden, Germany) according to the kit protocols.

16S/ITS rRNA amplicon sequencing (V3–V4 hypervariable region)

Quality checks were performed using the 2100 BioAnalyzer (Agilent Techologies Santa Clara, CA, USA), followed by library preparation with the NEBNext® Ultra™ II DNA Library Prep Kit (Illumina, San Diego, CA, USA). Sequencing was conducted on an Illumina NovaSeq 6000 with the following parameters: paired-end reads of 250 bp × 2 (PE250) and an output of 50,000 reads per sample. In silico analyses were performed on a Mac OS (Catalina version 10.15) terminal using Jupyter Notebook (Python version 3.9 version 6.4.11). Quality was assessed with FastQC (version 0.11.8). Data were analyzed using QIIME 2 (version 2023.7) with the Silva 138 99% OTUs full-length database (MD5: b8609f23e9b17bd4a1321a8971303310). The QIIME dada2 denoise-paired parameters were set as follows: --p-n-threads 0, --p-trim-left-f 30, --p-trim-left-r 30, --p-trunc-len-f 250, and --p-trunc-len-r 250. Operational taxonomic unit sequences were classified to determine the gut microbiota composition.

Bacterial abundance and identification

Body weights of 4 virgin adult females were measured following either darkness or BL irradiation. For Figure. 4B, after 3 days of BL irradiation followed by a 3-day recovery period, 4 surviving females aged 5–8 days were randomly chosen, immersed in 70% ethanol for 1 minute, washed three times with PBS homogenized in 500 µL of PBS in a 2-mL tube (stock solution), and diluted 1:10 with PBS. A 10-µL aliquot was plated onto an MRS agar plate (5.5 g MRS broth (Becton, Dickinson and Company, Franklin Lakes, NJ, USA), 1 g agar

(Fujifilm Wako Pure Chemicals Co.), and 100 mL distilled water). The plates were incubated for 72 hours at 30–31°C, and colony-forming units (CFU) were counted. Fold change values were calculated relative to the mean of the corresponding UCL replicate line (Figure. 4A); $\log_2$-fold change values were calculated relative to the mean of the corresponding non-treated UCL replicate line (Figure. 4B); fold change values were calculated relative to the mean of the corresponding UCL non-experience (Figure. 6a). Single bacterial colonies were isolated, and their 16S rRNA genes were amplified by PCR using universal bacterial primers 27F and 1492R. Sequencing was performed on an ABI3500 Sanger sequencing platform (Thermo Fisher Scientific) using the BigDye™ Terminator v1.1 Cycle Sequencing Kit (Thermo Fisher Scientific)[76,77].

Abx treatment

The Abx was prepared according to established protocols[78]; the diet was supplemented with 100 μg/mL streptomycin sulfate (Fujifilm Wako Pure Chemicals Co.), 50 μg/mL tetracycline hydrochloride (Fujifilm Wako Pure Chemicals Co.), and 200 μg/mL rifampicin (Fujifilm Wako Pure Chemicals Co.). Flies were reared on a diet containing Abx from the embryo stage to adult.

Capillary feeding (CAFE) assay

To prevent egg-laying within the capillaries, 4 virgin male flies aged 5–8 days were used. The assay was adapted from a previous study[79]. Flies were fed for 24 with a feeding solution (5% sucrose, 2% yeast extract, 0.25% nipagin in ethanol, and 0.005% red dye in water), and consumption was measured.

Infection with gut contents or *A. persici* cocktails

In Figure. 4D, Figure. S4B–D, Figure. 7C, and Figure. S6A, 30 virgin female flies aged 5–8 days were immersed in 70% ethanol for 1 minute, washes three times with PBS and

homogenized in 500 μL of PBS in a 2-mL tube (stock solution). The latter was diluted 1:10 with PBS. To infect with the gut microbiota, 20 μL of the diluted stock solution was added to the diet, and virgin females aged 1–4 days were maintained on this diet for 4 days. PBS was used as a control. Body weight was measured before and after infection. Climbing ability and fecundity were evaluated after 3 days of non-irradiation or BL irradiation followed by a 3-day recovery period. In Figure. S6B, *A. persici* was cultured and isolated on MRS plates for 48 hours. These isolates, along with the standard strain of *A. persici* (JCM 25330), were cultured in 200 μL of MRS broth (5.5 g MRS broth (Becton, Dickinson and Company) and 100 mL distilled water) in 96-well plates for 72 hours. Bacterial suspensions were centrifuged to obtain pellets, and the 10-μL bacterial culture pellet was diluted 1:30 with PBS and inoculated into 20 μL of diet. Autoclaved MRS was also diluted 1:30 with PBS, and 20 μL of this mixture was used as the control.

Whole-genome resequencing, variant identification, and enrichment analysis

Quality checks were performed using a BioAnalyzer, followed by library preparation with the NEBNext® Ultra DNA Library Prep Kit (Illumina). Sequencing was conducted on an Illumina NovaSeq 6000 with the following parameters: paired-end reads of 150 bp (PE150), a data output of 10 G bases per sample, and approximately 66.7 million reads per sample.

In silico analyses were performed using a macOS (Catalina version 10.15.7) terminal and Jupyter Notebook (Python version 3.9 version 6.4.11). The quality of the fastq files was assessed using seqkit stat (version 0.16.1) and then fastqc (version 0.11.8). Reads were trimmed using Trimmomatic (version 0.39) with the following parameters: LEADING:20, TRAILING:20, SLIDINGWINDOW:4:15, and MINLEN:20, based on Illumina adapter sequences (CTGTCTCTTATACACATCT). Trimmed reads were re-evaluated with seqkit stat and fastqc to confirm their quality.

Mapping was performed using the reference genome BDGP6.46, INSDC Assembly GCA_000001215.4 (details provided in Data S4). Indexing and mapping were conducted using bwa (version 0.7.17), followed by conversion from SAM to BAM format using samtools (version 1.10). PCR duplicates were marked with GATK (version 4.2.6.1), and alignment statistics were calculated from the BAM file. Paired-end reads were merged using samtools, and the merged BAM file was sorted.

Variants were called with sambamba mpileup and varScan pileup2snp, using the parameters: SNP; --min-coverage 10 --min-var-freq 0.90 --p-value 0.05 (filter; default), Indel; --min-coverage 10 --min-var-freq 0.90 --p-value 0.10 (filter; --min-reads2 4 --min-var-freq 0.15 --p-value 0.05). Homozygous variants were identified by extracting rows with matching Cons and VarAllele values. Common positions across replicates (lines 1, 2, and 3) within each strain were defined to identify strain-specific shared variants. Shared and unique variants among UCL, SL, and Canton-S (SRX8038113)[80] were analyzed.

Variants were annotated using SnpEff (version 5.0) and visualized using IGV (version 2.8.12). Enrichment analysis was conducted with ShinyGO 0.80 and KEGG, on the basis of the unique variants identified. Variants classified as having a low impact by SnpEff were excluded from the analysis list (full list available in Data S6).

RNA extraction

Ten virgin female flies aged 5–8 days were frozen in liquid nitrogen and homogenized in Trizol (Molecular Research Center, Inc., Cincinnati, OH, USA). Chloroform (Fujifilm Wako Pure Chemicals Co.) was then added, and the mixture was vortexed twice and centrifuged at 20,000 × *g* for 10 minutes at 4°C. The upper aqueous phase was transferred to a new tube, and 200 µL of isopropyl alcohol was added. The mixture was vortexed, incubated at room temperature for 10 minutes and centrifuged again at 20,000 × *g* for 10 minutes at 4°C; the supernatant was discarded. To wash the RNA pellet, 400 µL of 75% ethanol (prepared with DEPC-treated water) was added, followed by vortexing. The sample was then

centrifuged at 20,000 × *g* for 5 minutes at 4°C. The supernatant was discarded, and the pellet was centrifuged once more for 1 minute. The pellet was air-dried and resuspended in DEPC-treated water.

RNA-sequence and enrichment analysis

Quality assessment was initially performed using a BioAnalyzer. Library preparation was conducted with the NEBNext Ultra II Directional RNA Library Prep Kit (Illumina) and the NEBNext Poly(A) mRNA Magnetic Isolation Module (New England Biolabs, Ipswich, MA, USA). Sequencing was performed on an Illumina NovaSeq 6000, with a read length of PE150 (150 bp × 2 paired-end), generating a data output of 6 G bases per sample and approximately 40 million reads per sample.

In silico analyses and read trimming followed the protocols described in the "Whole-genome resequencing, variant identification, and enrichment analysis" section in Methods. Poly(A) tails were removed using cutadapt, and mapping was conducted with hisat2 (version 2.2.1) using the BDGP6.46 reference genome (INSDC Assembly GCA_000001215.4) (for details, see Data S4). Gene-wise read counting was accomplished using HTSeq (version 2.0.4) with the dmel-all-r6.54.gtf annotation file. Read counts were normalized with edgeR (version 3.40.2) using the trimmed mean of M values method. Subsequent principal component analysis and differential expression analysis were carried out with edgeR and scikit-learn (version 1.0.2). DEGs were identified by comparing non-treated SL with non-treated UCL, Abx-treated SL, or Abx-treated UCL groups, applying a false discovery rate–adjusted *p*-value threshold of <0.05. Python libraries such as pandas (version 2.0.3), numpy (version 1.25.2), scipy (version 1.11.2), and stats were used to filter DEGs with *p*-values below 0.05. For the DEGs, $\log_2$-fold change values and Z scores normalized within the range of −2 to 2 were calculated. These Z scores were then used to create a cluster map using the Ward method, which classified genes and treatments on the basis of their similarity patterns. Enrichment analysis was performed using ShinyGO 0.80. Gene lists related to specific

biological functions were retrieved from KEGG (for TCA cycle and oxidative phosphorylation) and FlyBase (for lipid metabolic processes).

In Figure. 5E, heatmaps illustrating functional profiles were generated using $\log_2$-fold change values. These values were compared for each gene and each group and normalized against the mean value of the non-treated UCL group.

Genetics and evaluation of TAG levels and BL tolerance

We collected genetically engineered flies with known elevated TAG levels and reared them at 23–25°C under a 12-hour light/dark cycle. Using the GAL4/UAS system and null mutants, we generated flies with RNAi knockdown or overexpression of target genes. The following strains from the Bloomington Stock Center were used (see Data S7):

Null mutants: *w;Akh* (BL84448), w;*Bmm* (BL15828), *yw,Pdgy* (BL19990), *yw;Chico* (BL14337), *w;InR* (BL8267), *w;Ilp 2 3 5* (BL30889), *w;Lk6* (BL87087)

GAL4 drivers: *yw;Lsp2* (BL6357), *w;ppl* (BL58768), *w;Tk* (BL51973)

UAS strains: *yv;UAS-AkhR*^{RNAi} (BL51710), *yv;UAS-Pect*^{RNAi} (BL63710), *yv;UAS-Pten*^{RNAi} (BL33643), *yv;UAS-Bmm*^{RNAi} (25926), *y sc v sev;UAS-Stim*^{RNAi} (BL52911), *y sc v sev;UAS-Lsd-1*^{RNAi} (BL65020), *yv;UAS-Tk*^{RNAi} (BL25800), *yw;UAS-Gbb* (BL63059), *yw;UAS-InR* (BL8263), *w;UAS-Lsd-2* (BL98116), *w;UAS-Lk6* (BL8709), *w,UAS-Rpr1* (BL5823)

We used F1 progenies for the experiments, obtained by crossing GAL4 driver males with UAS effector females. As controls, we used wild-type Canton-S and w1118 genetically washed by crossing with the Canton-S flies, F1 progenies from crosses of w1118 with UAS effectors, and F1 progenies from crosses of GAL4 drivers with *y sc v;eGFP*^{RNAi} (BL41555) and *y sc v;eGFP*^{RNAi} (BL41556) UAS effectors.

Virgin female flies aged 1–5 days were irradiated with either darkness or BL for 3 days and recovered for 3 days. Their survival rates were assessed, and 5 flies were randomly chosen to mate with 5 Canton-S males for 4 days (for details, see “Measurement of fecundity” in

Methods). TAG storage was measured in virgin female flies aged 7–12 days. Relative TAG levels are presented as $\log_2$-fold changes relative to the mean values across all treatments. Fecundity was calculated as $\log_2$-fold changes relative to the non-irradiation condition for each treatment. Data are from SL and UCL (replicate lines 1, generation 57).

Parental experience of BL irradiation

Flies were BL-irradiated for 3 days and recovered for 3 days. Randomly chosen males and females were allowed to mate and lay eggs for 4 days.

Statistical analysis

Bayesian state space model and estimation

In Figure. 2D, intergenerational fecundity data were analyzed using a Bayesian state space model implemented with pystan (Python 3.9, version 2.17.0.0). This model included the following components:

Data block: Defined the number of generations (length of the time series data), a vector of explanatory variables, and three outcome variables corresponding to each replicate line, each following a normal distribution.

Parameters block: Estimated a vector of levels with drift components (mu), vectors of random effects (r1, r2, r3), coefficients of the explanatory variables (b1, b2, b3), the standard deviation representing the magnitude of the drift component (s_z), and the standard deviations of the random effects (s_r1, s_r2, s_r3).

Transformed parameters block: Calculated the expected values for each outcome variable (lambda1, lambda2, lambda3) as the sum of the level with drift component (mu), the product of the explanatory variables' coefficients (b) and values (ex), and the random effects (r).

Model block: Assumed that the random effects followed a normal distribution with a mean of 0 and a given standard deviation. The state equation, mu[i] ~ normal(2 * mu[i-1] - mu[i-2], s_z), expressed changes in the level with drift components using a second-order local linear

regression. The observation equations, y1[i] ~ normal(lambda1[i], sigma1), y2[i] ~ normal(lambda2[i], sigma2), and y3[i] ~ normal(lambda3[i], sigma3), defined the observed values as following a normal distribution.

Generated quantities block: Sampled the predicted values for each outcome variable using the normal distribution rather than the Poisson log-link function.

Random numbers were generated according to the posterior distribution using the Markov Chain Monte Carlo (MCMC) method with parameters set to iter=10000, chains=4, and control={'adapt_delta': 0.8, 'max_treedepth': 20}. Convergence was confirmed by ensuring that the *R*hat of the predicted values was <1.10 and by examining the trace plots (for details, see Data S1).

Hierarchical Bayesian model

Unless otherwise specified, hierarchical uncertainty estimation, accounting for random effects, was performed using Hierarchical Bayesian Model (HBM). The model specification and execution used the following tools and versions:

Software: R (version 4.0.1), rstan (version 2.32.2, Stan version 2.26.1), brms (version 2.20.4), and bayesplot (version 1.10.0).

Bayesian model comparison: Conducted using Bayes Factor_{10} with the loo function, computing exp(0.5 * (elpd1 - elpd2)), where elpd1 denotes the model's expected log pointwise predictive density (elpd_loo) and elpd2 denotes that of the null model.

MCMC sampling: Parameters were set to seed=1, chains=4, iter=20000, warmup=5000, and thin=4. If convergence was not attained, adjustments were made to iter=25000 and warmup=10000, ensuring that *R*hat values remained below 1.10.

Prior distributions: Uniformly set to Gaussian.

Model details: Comprehensive details including the response variable, predictors, random effects, and estimation results are available in Data S1–5, 8–10. Results included posterior median estimates, Bayesian 95% credible intervals, and approximate *p*-values (*p*MCMC) computed from posterior sampling.

Posterior sampling and *p*MCMC calculation: To test whether the posterior distribution of the difference in each treatment was above or below 0, we followed references[81–84]. Posterior samplings of each parameter were stored in diff_samples, and pairwise comparisons of treatments were made using the formula: *p*MCMC = 2 * min(mean(diff_samples > 0), mean(diff_samples < 0)).

Correlation analysis

The Pearson correlation coefficient and confidence intervals were computed using the pearsonr function from the scipy.stats library.

References

1. Spitschan, M., Aguirre, G. K., Brainard, D. H. & Sweeney, A. M. Variation of outdoor illumination as a function of solar elevation and light pollution. *Sci. Rep.* **6**, 26756 (2016).
   DOI: 10.1038/srep26756
2. Song, B. M. & Lee, C. H. Toward a mechanistic understanding of color vision in insects. *Front. Neural Circuits* **12**, 16 (2018).
   DOI: 10.3389/fncir.2018.00016
3. Numata, H., Miyazaki, Y. & Ikeno, T. Common features in diverse insect clocks. *Zoological Lett.* **1**, 10 (2015).
   DOI: 10.1186/s40851-014-0003-y
4. Kavakli, I. H., Ozturk, N. & Gul, S. DNA repair by photolyases. *Adv Protein. Chem. Struct. Biol.* **115**, 1–19 (2019).
   DOI: 10.1016/bs.apcsb.2018.10.003
5. Shibuya, K., Onodera, S. & Hori, M. Toxic wavelength of blue light changes as insects grow. *PLoS One* **13**, e0199266 (2018).
   DOI: 10.1371/journal.pone.0199266
6. Hori, M., Shibuya, K., Sato, M. & Saito, Y. Lethal effects of short-wavelength visible light on insects. *Sci. Rep.* **4**, 7383 (2014).
   DOI: 10.1038/srep07383
7. Hori, M. & Suzuki, A. Lethal effect of blue light on strawberry leaf beetle, Galerucella grisescens (Coleoptera: Chrysomelidae). *Sci. Rep.* **7**, 2694 (2017).
   DOI: 10.1038/s41598-017-03017-z
8. Nash, T. R., Chow, E. S., Law, A. D., Fu, S. D., Fuszara, E., Bilska, A., Bebas, P., Kretzschmar, D & Giebultowicz, J. M. Daily blue-light exposure shortens lifespan and causes brain neurodegeneration in *Drosophila*. *NPJ Aging Mech. Dis.* **5**, 8 (2019).
   DOI: 10.1038/s41514-019-0038-6
9. Hall, H., Ma, J., Shekhar, S., Leon-Salas, W. D. & Weake, V. M. Blue light induces a neuroprotective gene expression program in *Drosophila* photoreceptors. *BMC Neurosci.* **19**, 43 (2018).
   DOI: 10.1186/s12868-018-0443-y
10. Yang, J., Song, Y., Law, A. D., Rogan, C. J., Shimoda, K., Djukovic, D., Anderson, J. C., Hendrix, D. A & Giebultowicz, J. M. Chronic blue light leads to accelerated aging in *Drosophila* by impairing energy metabolism and neurotransmitter levels. *Front. Aging* **3**, 983373 (2022).
    DOI: 10.3389/fragi.2022.983373
11. Song, Y., Yang, J., Law, A. D., Hendrix, D. A., Kretzschmar, D., Robinson, M & Giebultowicz, J. M. Age-dependent effects of blue light exposure on lifespan, neurodegeneration, and mitochondria physiology in *Drosophila melanogaster*. *NPJ Aging* **8**, 11 (2022).
    DOI: 10.1038/s41514-022-00092-z

12. Stanhope, S. C., Brandwine-Shemmer, T., Blum, H. R., Doud, E. H., Jannasch, A., Mosley, A. L., Minke, B & Weake, V. M. Proteome-wide quantitative analysis of redox cysteine availability in the *Drosophila melanogaster* eye reveals oxidation of phototransduction machinery during blue light exposure and age. *Redox Biol.* **63**, 102723 (2023).
DOI: 10.1016/j.redox.2023.102723
13. Scheiner, S. M. Selection experiments and the study of phenotypic plasticity. *J Evol. Biol.* **15**, 889–898 (2002).
DOI: 10.1046/j.1420-9101.2002.00468.x
14. Martínez, A. A. & Lang, G. I. Identifying targets of selection in laboratory evolution experiments. *J. Mol. Evol.* **91**, 345–355 (2023).
DOI: 10.1007/s00239-023-10096-2
15. Harshman, L. G. & Hoffmann, A. A. Laboratory selection experiments using *Drosophila*: what do they really tell us? *Trends Ecol. Evol.* **15**, 32-36 (2000).
DOI: 10.1016/S0169-5347(99)01756-5
16. Watson, M. J. O. & Hoffmann, A. A. Acclimation, cross-generation effects, and the response to selection for increased cold resistance in *Drosophila*. *Evolution* **50**, 1182-1192 (1996).
DOI: 10.1111/j.1558-5646.1996.tb02359.x
17. Sørensen, J. G., Schou, M. F. & Loeschcke, V. Evolutionary adaptation to environmental stressors: a common response at the proteomic level. *Evolution* **71**, 1627–1642 (2017).
DOI: 10.1111/evo.13243
18. Akhmetova, K., Balasov, M. & Chesnokov, I. *Drosophila* STING protein has a role in lipid metabolism. *eLife* **10**, e67358 (2021).
DOI: 10.7554/eLife.67358
19. Bailey, A. P., Koster, G., Guillermier, C., Hirst, E. M. A., MacRae, J. I., Lechene, C. P., Postle, A. D & Gould, A. P. Antioxidant role for lipid droplets in a stem cell niche of *Drosophila*. *Cell* **163**, 340–353 (2015).
DOI: 10.1016/j.cell.2015.09.020
20. Moulton, M. J., Barish, S., Ralhan, I., Chang, J., Goodman, L., Harland, J. G., Marcogliese, P. C., Johansson, J. O., Ioannou, M. S. & Bellen, H. J. Neuronal ROS-induced glial lipid droplet formation is altered by loss of Alzheimer's disease-associated genes. *Proc. Natl. Acad. Sci. UAS* **118**, e2112095118 (2021).
DOI: 10.1073/pnas.2112095118
21. Bastide, H., Yassin, A., Johanning, E. J. & Pool, J. E. Pigmentation in *Drosophila melanogaster* reaches its maximum in Ethiopia and correlates most strongly with ultra-violet radiation in sub-Saharan Africa. *BMC Evol. Biol.* **14**, 179 (2014).
DOI: 10.1186/s12862-014-0179-y
22. Zhao, S., Jang, C., Liu, J., Uehara, K., Gilbert, M., Izzo, L., Zeng, X., Trefely, S., Fernandez, S., Carrer, A., Miller, K. D., Schug, Z. T., Snyder, N. W., Gade, T. P., Rabinowitz, J. D. & Wellen, K. E. Dietary fructose feeds hepatic lipogenesis via

microbiota-derived acetate. *Nature* **579**, 586–591 (2020).
DOI: 10.1038/s41586-020-2101-7

23. Jugder, B. E., Kamareddine, L. & Watnick, P. I. Microbiota-derived acetate activates intestinal innate immunity via the Tip60 histone acetyltransferase complex. *Immunity* **54**, 1683-1697.e3 (2021).
DOI: 10.1016/j.immuni.2021.05.017

24. Paiva, P., Medina, F. E., Viegas, M., Ferreira, P., Neves, R. P. P., Sousa, J. P. M., Ramos, M. J. & Fernandes, P. A. Animal fatty acid synthase: a chemical nanofactory. *Chem. Rev.* **121**, 9502–9553 (2021).
DOI: 10.1021/acs.chemrev.1c00147

25. Miao, T., Kim, J., kang, P., Fujiwara, H., Hsu, FF & Bai, H. Acetyl-CoA-mediated autoacetylation of fatty acid synthase as a metabolic switch of de novo lipogenesis in *Drosophila*. *Proc. Natl. Acad. Sci. USA* **119**, e2212220119 (2022).
DOI: 10.1073/pnas.2212220119

26. Onuma, T., Yamauchi, T., Kosakamoto, H., Kadoguchi, H., Kuraishi, T., Murakami, T., Mori, H., Miura, M. & Obata, F. Recognition of commensal bacterial peptidoglycans defines *Drosophila* gut homeostasis and lifespan. *PLoS Genet.* **19**, e1010709 (2023).
DOI: 10.1371/journal.pgen.1010709

27. Chaston, J. M., Newell, P. D. & Douglas, A. E. Metagenome-wide association of microbial determinants of host phenotype in *Drosophila melanogaster*. *mBio* **5**, e01631-14 (2014).
DOI: 10.1128/mbio.01631-14

28. Newell, P. D. & Douglas, A. E. Interspecies interactions determine the impact of the gut microbiota on nutrient allocation in *Drosophila melanogaster*. *Appl. Environ. Microbiol.* **80**, 788–796 (2014).
DOI: 10.1128/AEM.02742-13

29. He, Y., Xie, Z., Zhang, H., Liebl, W., Toyama, H. & Chen, F. Oxidative fermentation of acetic acid bacteria and its products. *Front. Microbiol.* **13**, 879246 (2022).
DOI: 10.3389/fmicb.2022.879246

30. Shin, S. C., Kim, SH., You, H., Kim, B., Kim, A. C., Lee, KA., Yoon, JH., Ryu, JH. &Lee, WJ. *Drosophila* microbiome modulates host developmental and metabolic homeostasis via insulin signaling. *Science* **334**, 670–674 (2011).
DOI: 10.1126/science.1212782

31. Chaston, J. M., Dobson, A. J., Newell, P. D. & Douglas, A. E. Host genetic control of the microbiota mediates the *Drosophila* nutritional phenotype. *Appl. Environ. Microbiol.* **82**, 671–679 (2016).
DOI: 10.1128/AEM.03301-15

32. Gould, A. L., Zhang, V., Lamberti, L., Jones, E. W., Obadia, B., Korasidis, N., Gavryushkin, A., Carlson, J. M., Beerenwinkel, N. & Ludington, W. B. Microbiome interactions shape host fitness. *Proc. Natl. Acad. Sci. USA* **115**, E11951-E11960 (2018).
DOI: 10.1073/pnas.1809349115

33. Elgart, M., Stern, S., Salton, O., Gnainsky, Y., Heifetz, Y. & Soen, Y. Impact of gut microbiota on the fly's germ line. *Nat. Commun.* **7**, 11280 (2016).
DOI: https://doi.org/10.1038/ncomms11280

34. Henriques, S. F., Dhakan, D. B., Serra, L., Francisco, A. P., Carvalho-Santos, Z., Baltazar, C., Elias, A. P., Anjos, M., Zhang, T., Maddocks, O. D. K. & Ribeiro, C. Metabolic cross-feeding in imbalanced diets allows gut microbes to improve reproduction and alter host behaviour. *Nat. Commun.* **11**, 4236 (2020).
DOI: 10.1038/s41467-020-18049-9

35. Dodge, R., Jones, E. W., Zhu, H., Obadia, B., Martinez, D. J., Wang, C., Aranda-Díaz, A., Aumiller, K., Liu, Z., Voltolini, M., Brodie, E. L., Huang, K. C., Carlson, J. M., Sivak, D. A., Spradling, A. C. & Ludington, W. B. A symbiotic physical niche in *Drosophila melanogaster* regulates stable association of a multi-species gut microbiota. *Nat. Commun.* **14**, 1557 (2023).
DOI: 10.1038/s41467-023-36942-x

36. Broderick, N. A., Buchon, N. & Lemaitre, B. Microbiota-induced changes in *Drosophila melanogaster* host gene expression and gut morphology. *mBio* **5**, e01117-14 (2014).
DOI: 10.1128/mBio.01117-14

37. Yu, FX., Zhao, B. & Guan, KL. Hippo pathway in organ size control, tissue homeostasis, and cancer. *Cell* **163**, 811–828 (2015).
DOI: 10.1016/j.cell.2015.10.044

38. Li, Q., Nirala, N. K., Nie, Y., Chen, HJ., Ostroff, G., Mao, J., Wang, Q., Xu, L. & Ip, Y. T. Ingestion of food particles regulates the mechanosensing Misshapen-Yorkie pathway in *Drosophila* intestinal growth. *Dev. Cell* **45**, 433-449.e6 (2018).
DOI: 10.1016/j.devcel.2018.04.014

39. Huang, HL., Wang, S., Yin, MX., Dong, L., Wang, C., Lu, Y., Feng, M., Dai, C., Guo, X., Li, L., Zhao, B., Zhou, Z., Ji, H., Jiang, J., Zhao, Y., Liu, XY. & Zhang, L. Par-1 regulates tissue growth by influencing Hippo phosphorylation status and Hippo-Salvador association. *PLoS Biol.* **11**, e1001620 (2013).
DOI: 10.1371/journal.pbio.1001620

40. Li, Q., Li, S., Mana-Capelli, S., Flach, R. J. R., Danai, L. V., Amcheslavsky, A., Nie, Y., Kaneko, S., Yao, X., Chen, X., Cotton, J. L., Mao, J., McCollum, D., Jiang, J., Czech, M. P., Xu, L. & Ip, Y. T. The conserved Misshapen-Warts-Yorkie pathway acts in enteroblasts to regulate intestinal stem cells in *Drosophila*. *Dev. Cell* **31**, 291–304 (2014).
DOI: 10.1016/j.devcel.2014.09.012

41. Nyholm, L., Koziol, A., Marcos, S., Botnen, A. B., Aizpurua, O., Gopalakrishnan, S., Limborg, M. T., Gilbert, M. T. P. & Alberdi, A. Holo-omics: integrated host-microbiota multi-omics for basic and applied biological research. *iScience* **23**, 101414 (2020).
DOI: 10.1016/j.isci.2020.101414

42. Moschandrea, C., Kondylis, V., Evangelakos, I., Herholz, M., Schneider, F., Schmidt, C., Yang, M., Ehret, S., Heine, M., Jaeckstein, M. Y., Szczepanowska, K., Schwarzer,

R., Baumann, L., Bock, T., Nikitopoulou, E., Brodesser, S., Krüger, M., Frezza, C., Heeren, J., Trifunovic, A. & Pasparakis, M. Mitochondrial dysfunction abrogates dietary lipid processing in enterocytes. *Nature* **625**, 385–392 (2024). DOI: 10.1038/s41586-023-06857-0

43. Byrns, C. N., Perlegos, A. E., Miller, K. N., Jin, Z., Carranza, F. R., Manchandra, P., Beveridge, C. H., Randolph, C. E., Chaluvadi, V. S., Zhang, S. L., Srinivasan, A. R., Bennett, F. C., Sehgal, A., Adams, P. D., Chopra, G. & Bonini, N. M. Senescent glia link mitochondrial dysfunction and lipid accumulation. *Nature* **630**, 475–483 (2024). DOI: 10.1038/s41586-024-07516-8

44. Chatterjee, N. & Perrimon, N. What fuels the fly: energy metabolism in *Drosophila* and its application to the study of obesity and diabetes. *Sci. Adv.* **7**, eabg4336 (2021). DOI: 10.1126/sciadv.abg433

45. Heier, C. & Kühnlein, R. P. Triacylglycerol metabolism in *Drosophila melanogaster*. *Genetics* **210**, 1163–1184 (2018). DOI: 10.1534/genetics.118.301583

46. Song, W., Veenstra, J. A. & Perrimon, N. Control of lipid metabolism by Tachykinin in *Drosophila*. *Cell Rep.* **9**, 40–47 (2014). DOI: 10.1016/j.celrep.2014.08.060

47. Kamareddine, L., Robins, W. P., Berkey, C. D., Mekalanos, J. J. & Watnick, P. I. The *Drosophila* immune deficiency pathway modulates enteroendocrine function and host metabolism. *Cell Metab.* **28**, 449-462.e5 (2018). DOI: 10.1016/j.cmet.2018.05.026

48. Henry, L. P., Bruijning, M., Forsberg, S. K. G. & Ayroles, J. F. The microbiome extends host evolutionary potential. *Nat. Commun.* **12**, 5141 (2021). DOI: 10.1038/s41467-021-25315-x

49. Henry, L. P. & Ayroles, J. F. Meta-analysis suggests the microbiome responds to evolve and resequence experiments in *Drosophila melanogaster*. *BMC Microbiol.* **21**, 108 (2021). DOI: 10.1186/s12866-021-02168-4

50. Bruijning, M., Henry, L. P., Forsberg, S. K. G., Metcalf, C. J. E. & Ayroles, J. F. Natural selection for imprecise vertical transmission in host–microbiota systems. *Nat. Ecol. Evol.* **6**, 77–87 (2022). DOI: 10.1038/s41559-021-01593-y

51. Henry, L. P., Fernandez, M., Webb, A. & Ayroles, J. F. Host evolutionary history and ecological context modulate the adaptive potential of the microbiome. Preprint at https://doi.org/10.1101/2020.09.21.306779 (2020).

52. Liu, L., Zhang, K., Sandoval, H., Yamamoto, S., Jaiswal., M., Sanz, E., Li, Z., Hul, J., Graham, B. H., Quintana, A. & Bellen, H. J. Glial lipid droplets and ROS induced by mitochondrial defects promote neurodegeneration. *Cell* **160**, 177–190 (2015). DOI: 10.1016/j.cell.2014.12.019

53. Reiff, T., Jacobson, J., Cognigni, P., Antonello, Z., Ballesta, E., Junn, Tan, K. J., Yew, J. Y., Dominguez, M. & Miguel-Aliaga, I. Endocrine remodelling of the adult intestine

sustains reproduction in *Drosophila. eLife* **4**, e06930 (2015).
DOI: 10.7554/eLife.06930

54. Buszczak, M., Lu, X., Segraves, W. A., Chang, T. Y. & Cooley, L. Mutations in the Midway gene disrupt a *Drosophila* Acyl Coenzyme A: diacylglycerol acyltransferase. *Genetics* **160**, 1511-1518 (2002).
DOI: 10.1093/genetics/160.4.1511

55. Murphy, M. P. How mitochondria produce reactive oxygen species. *Biochem. J.* **417**, 1–13 (2009).
DOI: 10.1042/BJ20081386

56. Crotti, E., Rizzi, A., Chouaia, B., Ricci, I., Favia, G., Alma, A., Sacchi, L., Bourtzis, K., Mandrioli, M., Cherif, A., Bandi, C. & Daffonchio, D. Acetic acid bacteria, newly emerging symbionts of insects. *Appl. Environ. Microbiol.* **76**, 6963–6970 (2010).
DOI: 10.1128/AEM.01336-10

57. Shi, L. & Tu, B. P. Acetyl-CoA and the regulation of metabolism: mechanisms and consequences. *Curr. Opin. Cell Biol.* **33**, 125–131 (2015).
DOI: 10.1016/j.ceb.2015.02.003

58. Li, X. & Karpac, J. A distinct Acyl-CoA binding protein (ACBP6) shapes tissue plasticity during nutrient adaptation in *Drosophila*. *Nat. Commun.* **14**, 7599 (2023).
DOI: 10.1038/s41467-023-43362-4

59. Narita, T., Weinert, B. T. & Choudhary, C. Functions and mechanisms of non-histone protein acetylation. *Nat. Rev. Mol. Cell Biol.* **20**, 156-174 (2019).
DOI: 10.1038/s41580-018-0081-3

60. Fitz-James, M. H. & Cavalli, G. Molecular mechanisms of transgenerational epigenetic inheritance. *Nat. Rev. Genet.* **23**, 325–341 (2022).
DOI: 10.1038/s41576-021-00438-5

61. Huang, J., Zhou, F., Zhou, H., Zheng, X., Huo, Z., Yang, M., Xu, Z., Liu, R., Wang, L. & Wang, X. Systematic assessment of transcriptomic and metabolic reprogramming by blue light exposure coupled with aging. *PNAS Nexus* **2**, 1-15(2023).
DOI: 10.1093/pnasnexus/pgad390

62. Christensen, C. F., Laurichesse, Q., Loudhaief, R., Colombani, J. & Andersen, D. S. *Drosophila* activins adapt gut size to food intake and promote regenerative growth. *Nat. Commun.* **15**, 273 (2024).
DOI: 10.1038/s41467-023-44553-9

63. Nagai, H., Nagai, L. A. E., Tasaki, S., Nakato, R, Umetsu, D., Kuranaga, E., Miura, M. & Nakajima, Y. Nutrient-driven dedifferentiation of enteroendocrine cells promotes adaptive intestinal growth in *Drosophila*. *Dev. Cell* **58**, 1764-1781.e10 (2023).
DOI: 10.1016/j.devcel.2023.08.022

64. Karasov, W. H., Martínez Del Rio, C. & Caviedes-Vidal, E. Ecological physiology of diet and digestive systems. *Annu. Rev. Physiol.* **73**, 69–93 (2011).
DOI: 10.1146/annurev-physiol-012110-142152

65. Stojanović, O., Miguel-Aliaga, I. & Trajkovski, M. Intestinal plasticity and metabolism as regulators of organismal energy homeostasis. *Nat. Metab.* **4**, 1444–1458 (2022).

DOI: 10.1038/s42255-022-00679-6

66. Miguel-Aliaga, I., Jasper, H. & Lemaitre, B. Anatomy and physiology of the digestive tract of *Drosophila melanogaster*. *Genetics* **210**, 357–396 (2018).
DOI: 10.1534/genetics.118.300224

67. Chevalier, C., Stojanović, O., Colin, D. J., Suarez-Zamorano, N., Tarallo, V., Veyrat-Durebex, C., Rigo, D., Fabbiano, S., Stevanović, A., Hagemann, S., Montet, X., Seimbille, Y., Zamboni, N., Hapfelmeier, S. & Trajkovski, M. Gut microbiota orchestrates energy homeostasis during cold. *Cell* **163**, 1360–1374 (2015).
DOI: 10.1016/j.cell.2015.11.004

68. Buchon, N., Osman, D., David, F. P. A., Fang, H. Y., Boquete, JP., Deplancke, B. & Lemaitre, B. Morphological and molecular characterization of adult midgut compartmentalization in *Drosophila*. *Cell Rep.* **3**, 1725–1738 (2013).
DOI: 10.1016/j.celrep.2013.04.001

69. Torquato, L. S., Mattos, D., Matta, B. P. & Bitner-Mathé, B. C. Cellular basis of morphological variation and temperature-related plasticity in *Drosophila melanogaster* strains with divergent wing shapes. *Genetica* **142**, 495–505 (2014).
DOI: 10.1007/s10709-014-9795-0

70. Lee, J. H., Bassel-Duby, R. & Olson, E. N. Heart- and muscle-derived signaling system dependent on MED13 and Wingless controls obesity in *Drosophila*. *Proc. Natl. Acad. Sci. USA* **111**, 9491–9496 (2014).
DOI: 10.1073/pnas.1409427111

71. Bligh. E. G & Dyer. W. J. A rapid method of total lipid extraction and purification. *Can. J. Biochem. Physiol.* **37**, 911-7 (1959).
DOI: 10.1139/o59-099

72. Guan, X. L., Cestra, G., Shui, G., Kuhrs, A., Schittenhelm, R. B., Hafen, E., van der Goot, F. G., Robinett, C. C., Gatti, M., Gonzalez-Gaitan, M. & Wenk, M. R. Biochemical membrane lipidomics during *Drosophila* development. *Dev. Cell* **24**, 98–111 (2013).
DOI: 10.1016/j.devcel.2012.11.012

73. Shen, L. R., Lai, C. Q., Feng, X., Parnell, L. D., Wan, J. B., Wang, J. D., Li, D., Ordovas, J. M. & Kang, J. X. *Drosophila* lacks C20 and C22 PUFAs. *J. Lipid Res.* **51**, 2985–2992 (2010).
DOI: 10.1194/jlr.M008524

74. Wood, J. G., Schwer, B., Wickremesinghe, P. C., Hartnett, D. A., Garcia, M., Li, M., Verdin, E. & Helfand, S. L. Sirt4 is a mitochondrial regulator of metabolism and lifespan in *Drosophila melanogaster*. *Proc. Natl. Acad. Sci. USA* **115**, 1564–1569 (2018).
DOI: 10.1073/pnas.172067311

75. Ward, J. H. Hierarchical grouping to optimize an objective function. *J. Am. Stat. Assoc.* **58**, 236-244 (1963).
DOI: 10.1080/01621459.1963.10500845

76. Weisburg, W. G., Barns, S. M., Pelletier, D. A. & Lane, D. J. 16S Ribosomal DNA

amplification for phylogenetic study. *J. Bacteriol.* **173**, 697-703 (1991).
DOI: 10.1128/jb.173.2.697-703.1991

77. Edwards, U., Rogall, T., Blöcker, H., Emde, M. & Böttger, E. C. Isolation and Direct Complete Nucleotide Determination of Entire Genes. Characterization of a Gene Coding for 16S Ribosoma] RNA. *Nucleic Acids Res.* **17**, 7843-7853 (1989).
DOI: 10.1093/nar/17.19.7843

78. Leftwich, P. T., Clarke, N. V. E., I. Hutchings, M. & Chapman, T. Gut microbiomes and reproductive isolation in *Drosophila*. *Proc. Natl. Acad. Sci. USA* **114**, 12767-12772 (2017).
DOI: 10.1073/pnas.1708345114

79. Kanno, M., Hiramatsu, S., Kondo, S., Tanimoto, H. & Ichinose, T. Voluntary intake of psychoactive substances is regulated by the dopamine receptor Dop1R1 in *Drosophila*. *Sci. Rep*. **11**, 3432 (2021).
DOI: 10.1038/s41598-021-82813-0

80. Wierzbicki, F., Schwarz, F., Cannalonga, O. & Kofler, R. Novel quality metrics allow identifying and generating high-quality assemblies of piRNA clusters. *Mol. Ecol. Resour.* **22**, 102–121 (2022).
DOI: 10.1111/1755-0998.13455

81. Bürkner, P. C. brms: An R package for Bayesian multilevel models using Stan. *J. Stat. Softw.* **80**, 1-28 (2017).
DOI: 10.18637/jss.v080.i01

82. Nott, D. J., Drovandi, C. C., Mengersen, K. & Evans, M. Approximation of Bayesian predictive *p*-values with regression ABC. *Bayesian Anal.* **13**, 59–83 (2018).
DOI: 10.1214/16-BA1033

83. Cornwallis, C. K., van't Padje, A., Ellers, J., Klein, M., Jackson, R., Kiers, E. T., West, S. A. & Henry L. M. Symbioses shape feeding niches and diversification across insects. *Nat. Ecol. Evol.* **7**, 1022–1044 (2023).
DOI: 10.1038/s41559-023-02058-0

84. Hadfield, J. D. MCMC methods for multi-response generalized linear mixed models: The MCMCglmm R package. *J. Stat. Softw.* **33**, 1-22 (2010).
DOI: 10.18637/jss.v033.i02

Acknowledgements

We are grateful to Dr. Takema Fukatu, Dr. Yuto Yoshinari, Dr. Takashi Nishimura, and Dr. Koichiro Tamura for their valuable discussions regarding the study. We also thank Dr. Masaki Iwata, Dr. Shuhei Miyashita, Dr. Chisato Kobayashi, Dr. Yuma Takahashi, Dr. Takahisa Ueno, Dr. Masashi Murakami, and Dr. Sota Tanaka for their important suggestions. We would like to thank Dr. Atsuhiko Nagasawa and Mr. Yuki Chiba for teaching us the GC-MS analysis, and Dr. Fu Namai for teaching us microbiome analysis. We also thank Mr. Yusaku Hayashi for instructing us on how to dissect the fat body. Ms. Ayako Abe and Mr. Kento Fukuoka provided technical assistance. We extend our gratitude to Dr. Haruki Kitazawa and Dr. Shoichiro Kurata for lending us their laboratories. We thank the Rhelixa, Inc. for conducting the next-generation sequencing and assisting with the data acquisition, ELSS, Inc for proofreading and editing the English language of this manuscript, Bloomington Drosophila Stock Center for providing the *Drosophila* stocks used in this study, and Japan Collection of Microorganisms RIKEN BioResource Research Center for providing the bacterial strains used in this research.

This work was supported by JST SPRING, grant numbers JPMJSP2102 and JPMJSP2114 to Y.T.

Author information

Authors and Affiliations

Graduate School of Agricultural Sciences, Tohoku University, Sendai, Japan

Yuta Takada, Wakako Ikeda-Ohtsubo, and Masatoshi Hori

Frontier Research Institute for Interdisciplinary Sciences, Tohoku University, Sendai, Japan

Toshiharu Ichinose

Graduate School of Pharmaceutical Sciences, Tohoku University, Sendai, Japan

Naoyuki Fuse

Graduate School of Life Sciences, Tohoku University, Sendai, Japan

Toshiharu Ichinose, Kokoro Saito, and Hiromu Tanimoto

Contributions

Y.T. and M.H. conceived and designed the study. Y.T. performed all experiments and analyzed all data, wrote the original manuscript and third manuscripts. Y.T. and W.I. designed and performed the infection experiment with gut contents and bacterial experiments. Y.T., T.I., and N.F. performed whole-genome and RNA sequencing. Y.T., K.S., T.I., and H.T. designed the genetic and CAFE assays. Y.T. and K.S. performed the CAFE assay. Y.T., W.I., N.F., and T.I. edited the first manuscript. Y.T. and T.I. edited the second manuscript. H.T. and M.H. supervised the study. All authors participated in the discussions and reviewed the manuscript.

There are no conflicts of interest to declare in relation to this study.

Figures

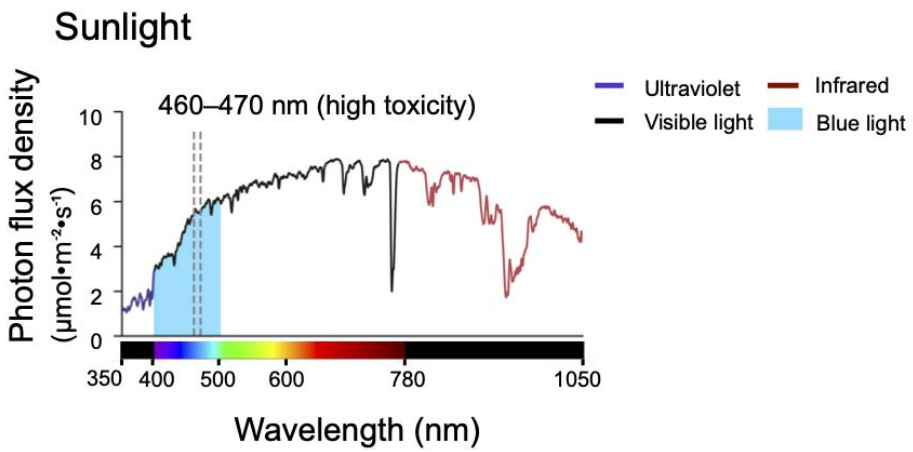

Figure. 1 | Sunlight contains a significant amount of blue light.

Sunlight photon flux density: Sendai, Japan; 38°N, 140°E, clear sky; November 21, 2021; 11:30 AM (approximately 4000 μmol·m^{-2}·s^{-1}, blue light: approximately 470 μmol·m^{-2}·s^{-1}). 460–470 nm is a highly toxic wavelength range for *Drosophila* adults. For details, see Data S1.

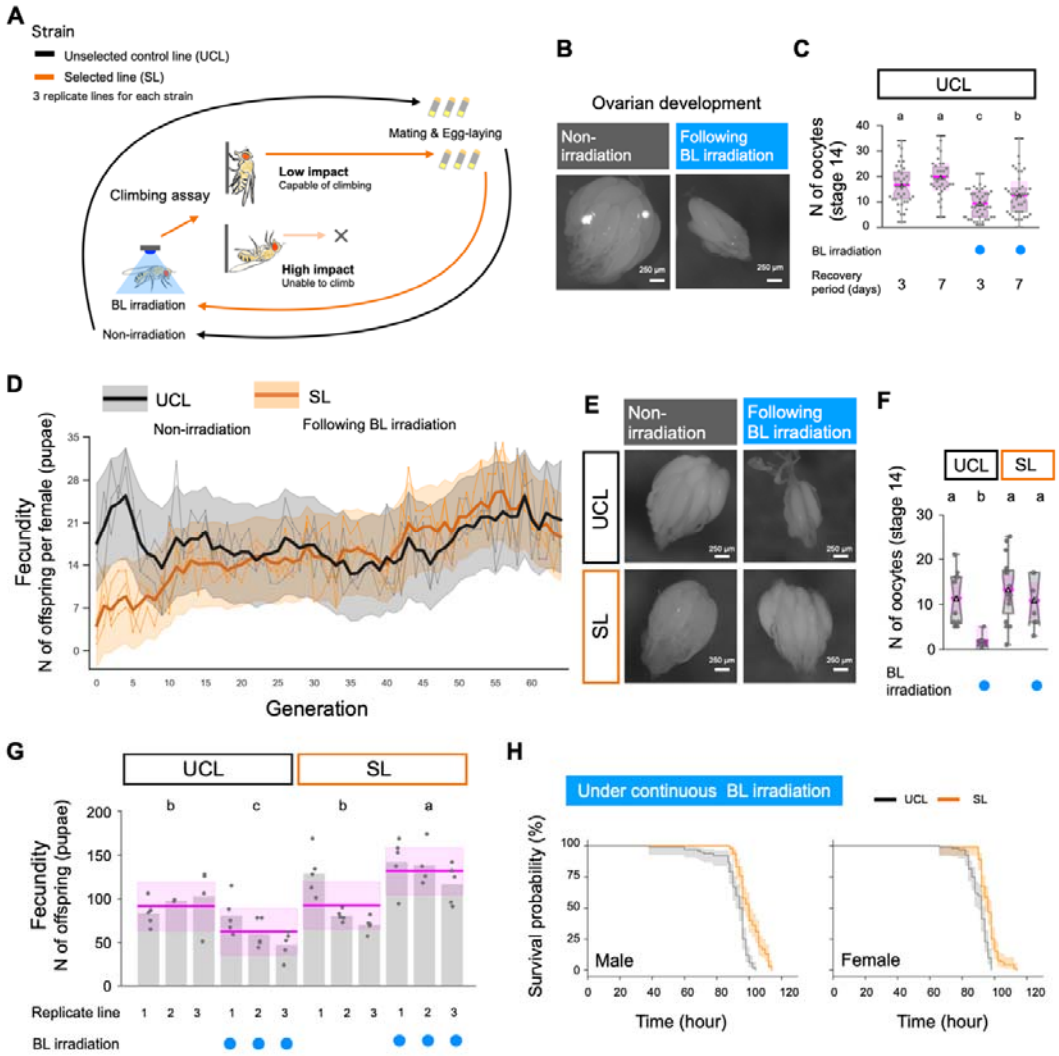

Figure. 2 | Establishment of *Drosophila* lines with blue light (BL) tolerance evolved by laboratory selection.

A, Experimental design of laboratory selection using BL toxicity. Flies were BL-irradiated for 3 days, recovered for 2 days, and categorized in a climbing assay into those capable of climbing ("low impact") and those unable to climb ("high impact"). Flies from the "low impact" group (selected lines, SL) were allowed 5 days for mating and egg-laying. Unselected control line (UCL) parents were randomly chosen from the negative control group and reared under the same conditions as the SL flies. **B**, **C**, Impact of BL toxicity on UCL flies (generation 34) subjected to a single irradiation for 3 days: (**B**) ovarian development, (**C**) the

number of stage 14 oocytes after recovery. n = 34–42. Bayes factor $(BF)_{10} > 100$. **D**, Changes in fecundity across generations. Fecundity was measured as the number of offspring per female (pupae). n = 3. Bayesian state space model with Markov Chain Monte Carlo (MCMC) method, posterior median and Bayesian 95% credible intervals (CI). **E**, Ovarian development differences after 3 days of BL irradiation followed by 3 days of recovery. **f**, Number of stage 14 oocytes after a 3-day recovery period. n = 9–15. BF_{10} = 50.74. (Replicate lines 2, generation 25). **G**, Fecundity measured as the number of offspring (pupae). n = 11–15. BF_{10} = 50.74, generation 38. **H**, Lifespan under continuous BL irradiation. Male n = 100. BF_{10} >100. Estimates: UCL 90.62 h (89.38–91.82), SL 96.35 h (95.16–97.52), pMCMC < 0.001. Female n = 92. BF_{10} = 0.72. Estimates: UCL 92.09 h (90.38–93.78), SL 100.39 h (98.74–102.13), pMCMC < 0.001. (Replicate lines 1, generation 25).

Statistical analyses for panels **C**, **F**, **G**, **H** used a Hierarchical Bayesian Model (HBM) with MCMC methods, posterior median, and Bayesian 95% CI. In **C**, **F**, and **G**, different letters indicate significant differences at pMCMC < 0.05 (see also Data S1).

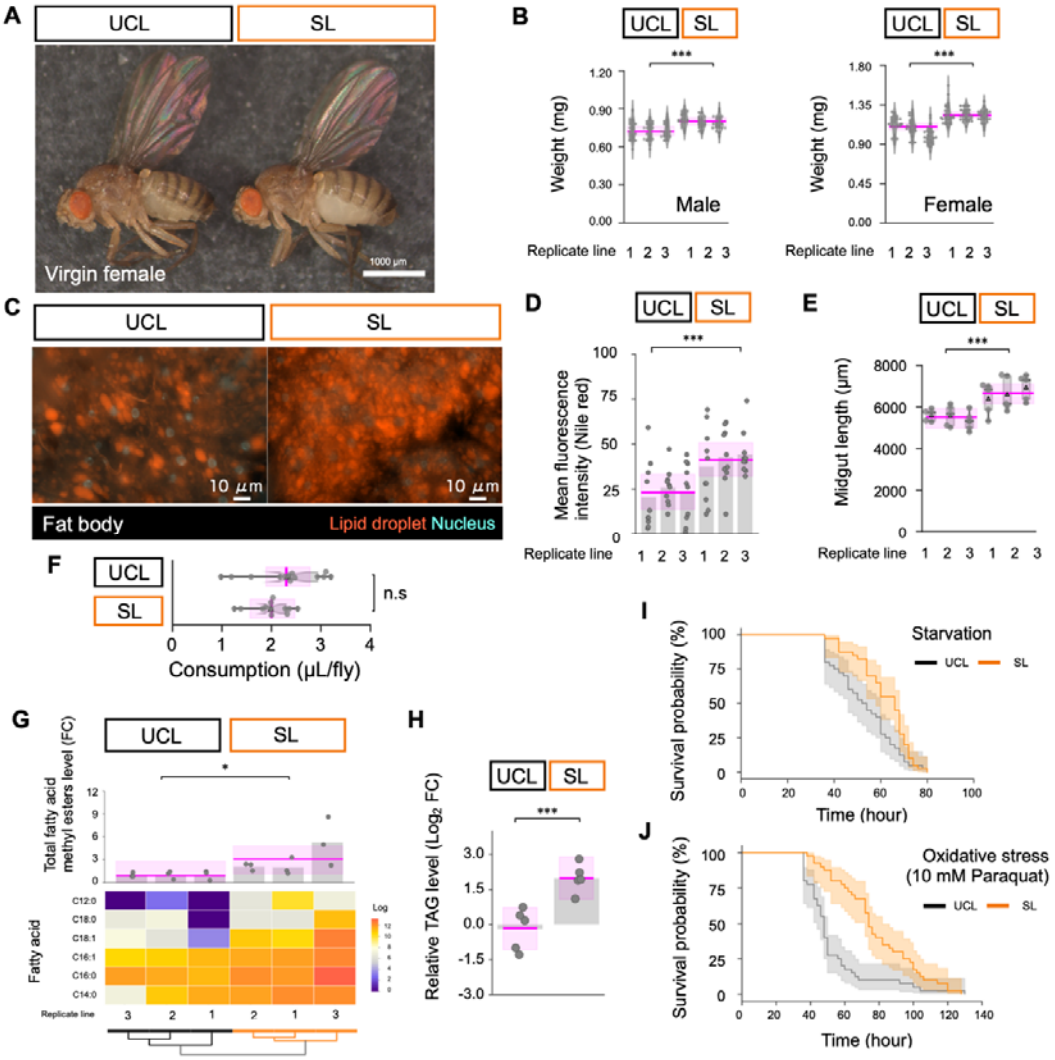

Figure. 3 | SL flies exhibited obese phenotype, lipid accumulation, and oxidative stress resistance.

A, Phenotype of adult virgin females aged 6–8 days. **B**, Body weight, n = 90, BF_{10} >100, generation 39. **C**, Fluorescence imaging of the abdominal fat body and lipid droplets (lipid droplets: Nile red; nuclei: NucBlue). **D**, Mean fluorescence intensity from Nile red staining, n = 30, BF_{10} >100, generation 35. **E**, Midgut length, n = 15, BF_{10} >100, generation 45. **F**, Food consumption, n = 12–13, BF_{10} = 1.85, replicate line 1, generation 52. **G**, Gas chromatography mass spectrometry analyses of fatty acid methyl esters (FAMEs), total FAMEs, n = 9, BF_{10} = 1.69, generation 30. **H**, Relative triacylglycerol (TAG) level, n = 5, BF_{10}

=15.14, replicate line 1, generation 57. **I**, Starvation resistance, Kaplan–Meier survival curve, *n* = 40, BF_{10} = 4.49. Estimates: UCL 53.04 h (49.20–56.89), SL 61.91 h (58.09–65.43), replicate line 2, generation 43. **J**, Oxidative stress resistance (10 mM paraquat), Kaplan–Meier survival curve, *n* = 40, BF_{10} >100. Estimates: UCL 53.07 h (45.90–59.03), SL 77.94 h (71.19–84.08), replicate line 3, generation 43. Statistical analyses for panels **B**, **D**, **E**, **F**, **G**, **H**, **I,** and **J** were performed using a HBM with MCMC methods, posterior median, and Bayesian 95% CI. Asterisks indicate significance levels: * *p*MCMC < 0.05, *** *p*MCMC < 0.001, n.s = not significant (see also Data S2). FC, fold change.

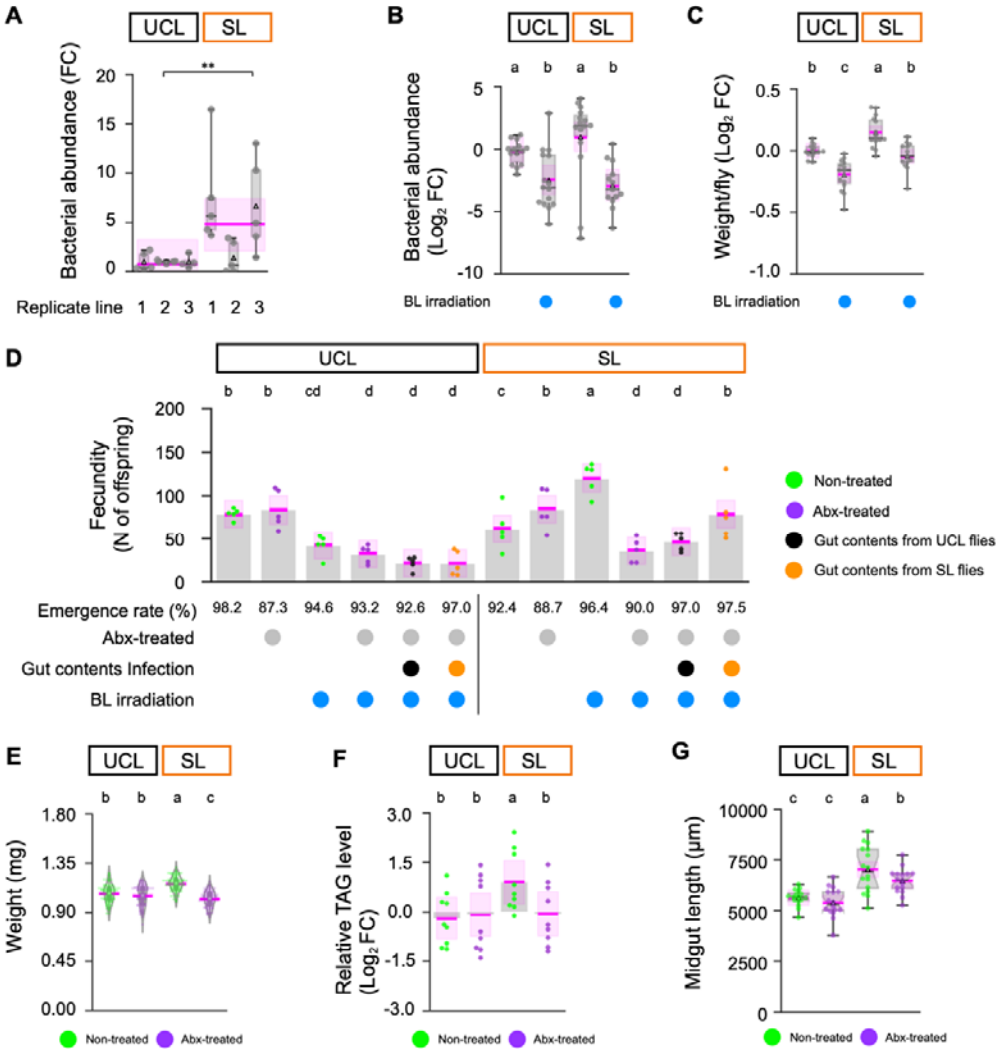

Figure. 4 | High bacterial abundance is the key to BL tolerance and lipid accumulation in SL flies.

A, Bacterial abundance, n = 15, BF_{10} = 9.22. Asterisks indicate significance: ** pMCMC < 0.01; generation 38. **B**, Bacterial abundance, n = 13–15, BF_{10} >100; generation 38. **C**, Body weight, n = 16, BF_{10} >100; generation 38. **D,** Fecundity measured as the number of offspring (adults), n = 5, BF_{10} >100; replicate line 1, generation 47. **E**, Body weight, n = 100, BF_{10} >100; replicate line 1, generation 55. **F**, Relative TAG level, n = 10, BF_{10} = 1.47; replicate line 1, generation 55. **G,** Midgut length, n = 16, BF_{10} >100; replicate line 1, generation 48. Statistical analyses for panels **B**–**G** were performed using a HBM with MCMC methods,

posterior median, and Bayesian 95% CI. Different letters indicate significant differences at *p*MCMC < 0.05 (see also Data S3).

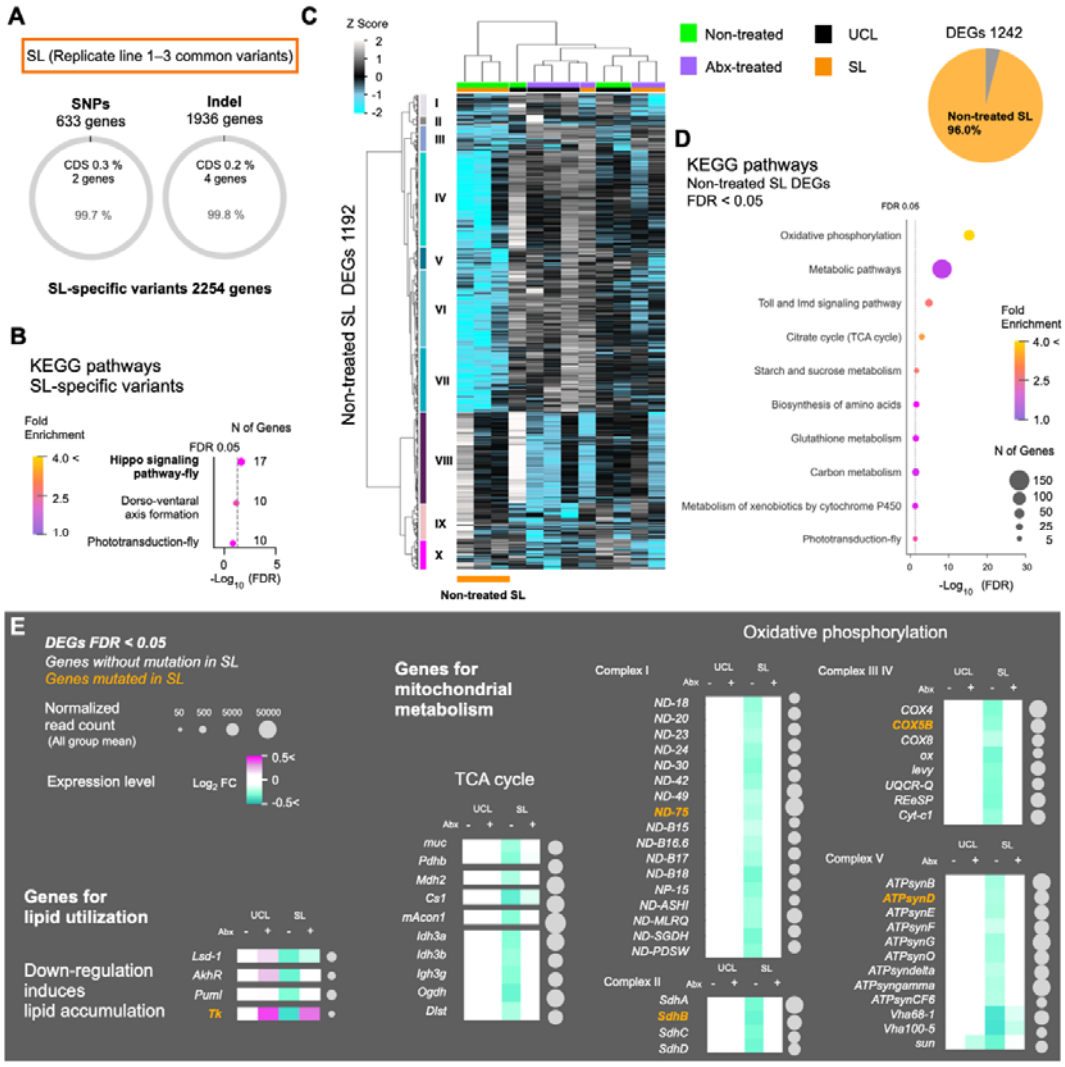

Figure. 5 | Host genome and transcriptomic profiles explain the characteristic phenotype of SL flies.

A, Identification of SL-specific variants through whole-genome resequencing; generation 44. CDS, coding sequence. **B**, Enrichment analysis of SL-specific variants using Kyoto Encyclopedia of Genes and Genomes (KEGG) with a false discovery rate (FDR)–adjusted *p*-value threshold of <0.05. **C**, Cluster map of differentially expressed genes (DEGs); replicate line 1, generation 50. **D**, Enrichment analysis of non-treated SL DEGs using KEGG with an FDR-adjusted *p*-value threshold of <0.05. **E**, Heatmaps illustrating functional profiles. All genes shown are DEGs (FDR < 0.05). For details, see Data S6.

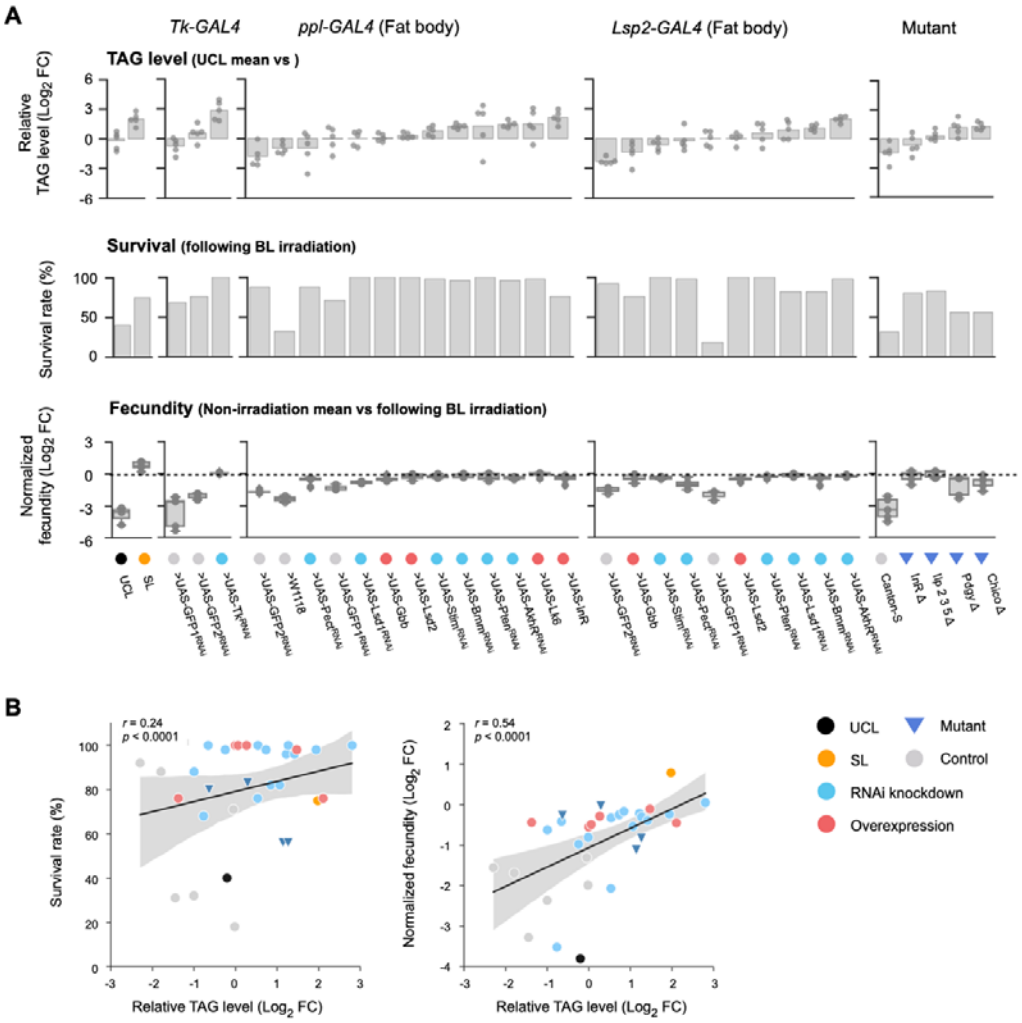

Figure. 6 | Lipid accumulation via genetic manipulation confers BL tolerance.

A, Relative TAG levels, survival rates following BL irradiation, and normalized fecundity. **B**, Correlation analysis. See also Data S7.

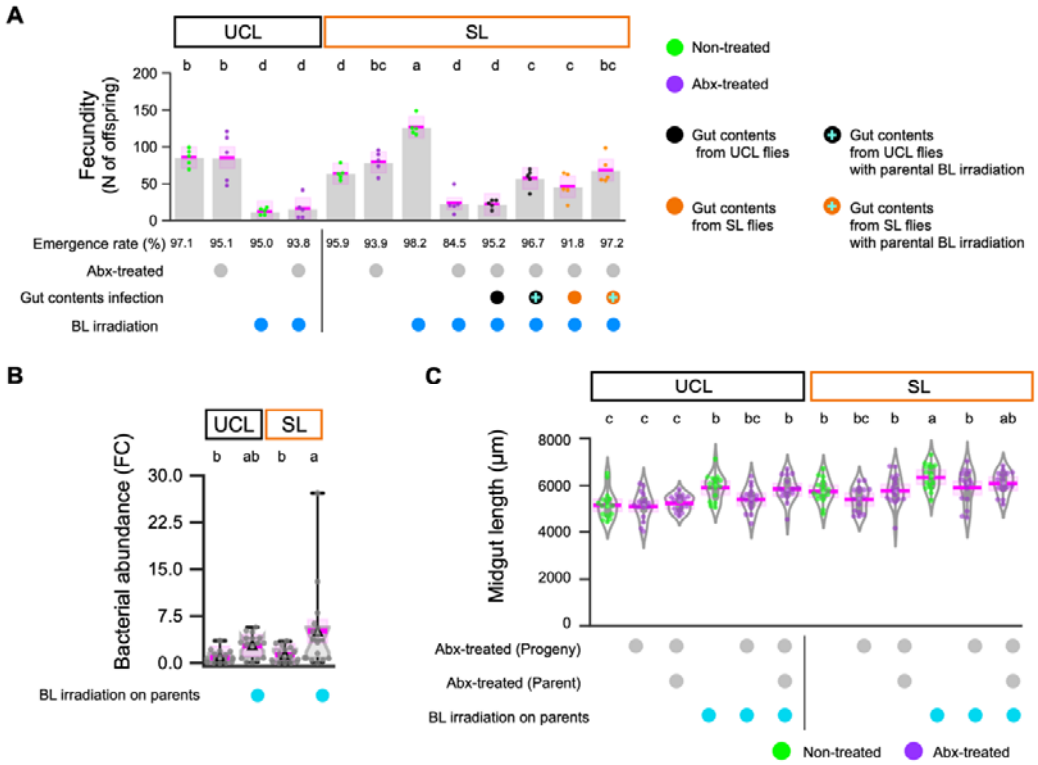

Figure. 7 | Parental experience of BL irradiation promotes midgut elongation and increased bacterial abundance in progeny.

A, Fecundity: number of offspring (adults). *n* = 5. BF_{10} >100; replicate line 1, generation 53. **B**, Bacterial abundance. *n* = 16. BF_{10} = 63.02; replicate line 1, generation 53. **C**, Midgut length. *n* = 16, BF_{10} >100; replicate line 1, generation 54.

Statistical analyses for panels **A**–**C** were performed using HBM with MCMC methods, posterior median, and Bayesian 95% CI. Different letters indicate significant differences at *p*MCMC < 0.05. For details, see Data S9 for all results, including statistical models.

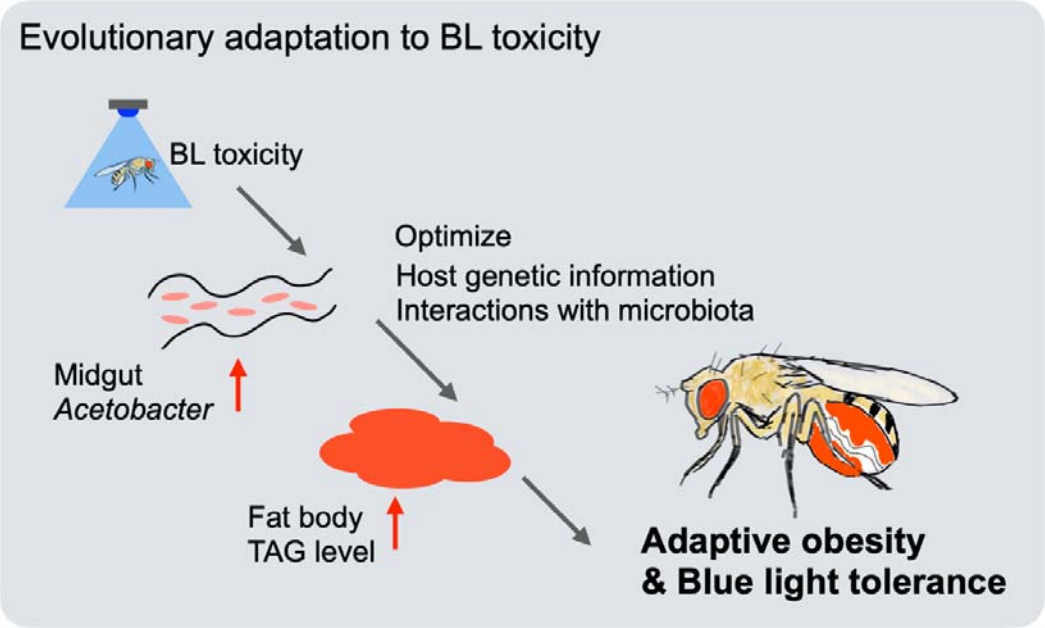

Figure. 8 | Gut microbiota–mediated obesity drives evolutionary adaptation to BL toxicity.

Evolutionary adaptation to BL toxicity involves selective pressure and the intergenerational transmission of parental experience, which drives midgut elongation, increased bacterial abundance, and optimization of both host genetic information and microbiota interaction. These changes can alter gene expression related to lipid metabolism, facilitating the formation of adaptive obesity characterized by lipid accumulation via the gut microbiota.

Supplementary Figures

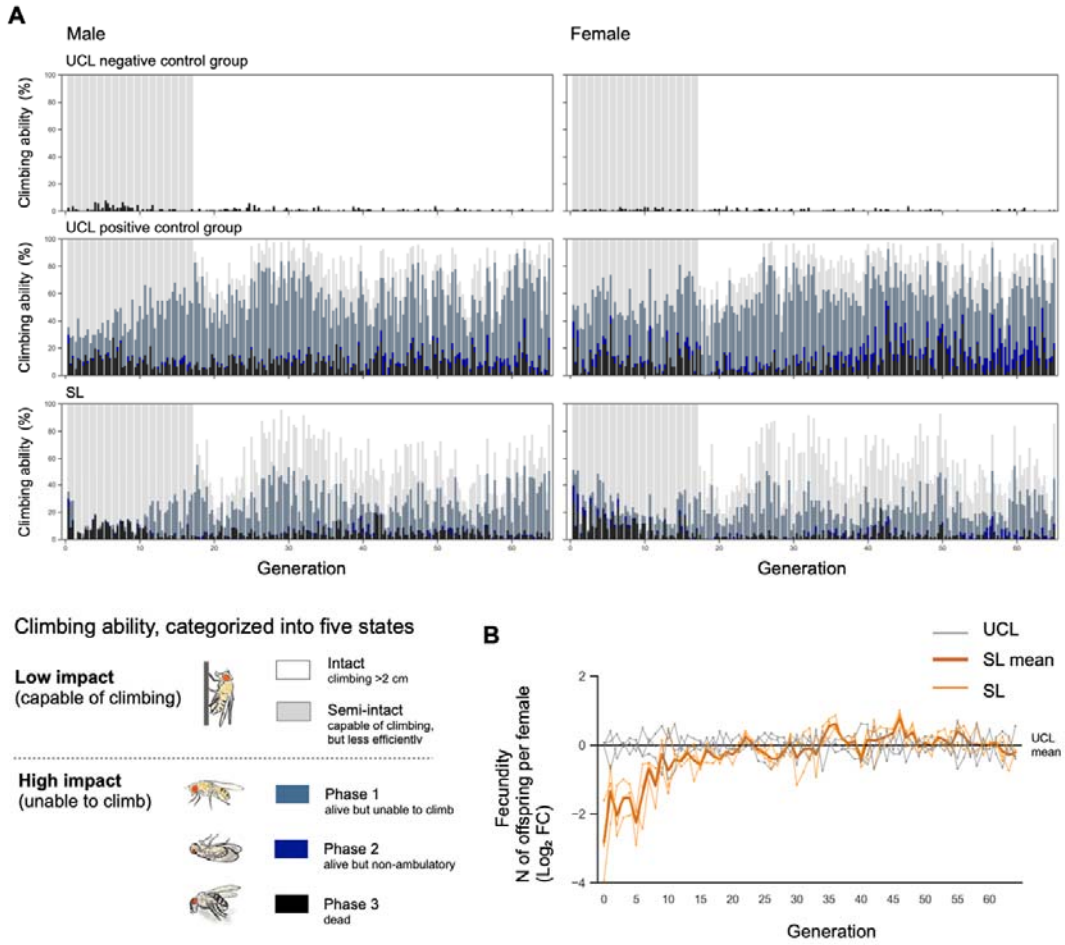

Figure. S1 | SL flies are BL tolerant.

A, Climbing ability and generational changes in male and female flies after exposure to BL irradiation. Climbing ability is represented by a total of 60–100 flies per bar, with bars representing replicate lines 1, 2, and 3. All categories were exposed to BL except the negative control group (top). Negative control group: The UCL flies were kept in darkness for 3 days instead of BL irradiation. Positive control group: A subset of UCL flies in each generation was exposed to BL under the same conditions as SL. **B,** Changes in fecundity across generations resulting from laboratory selection. The number of offspring per female (pupae) is shown. Data from Figure. 2D were Log_2-transformed relative to the average UCL value.

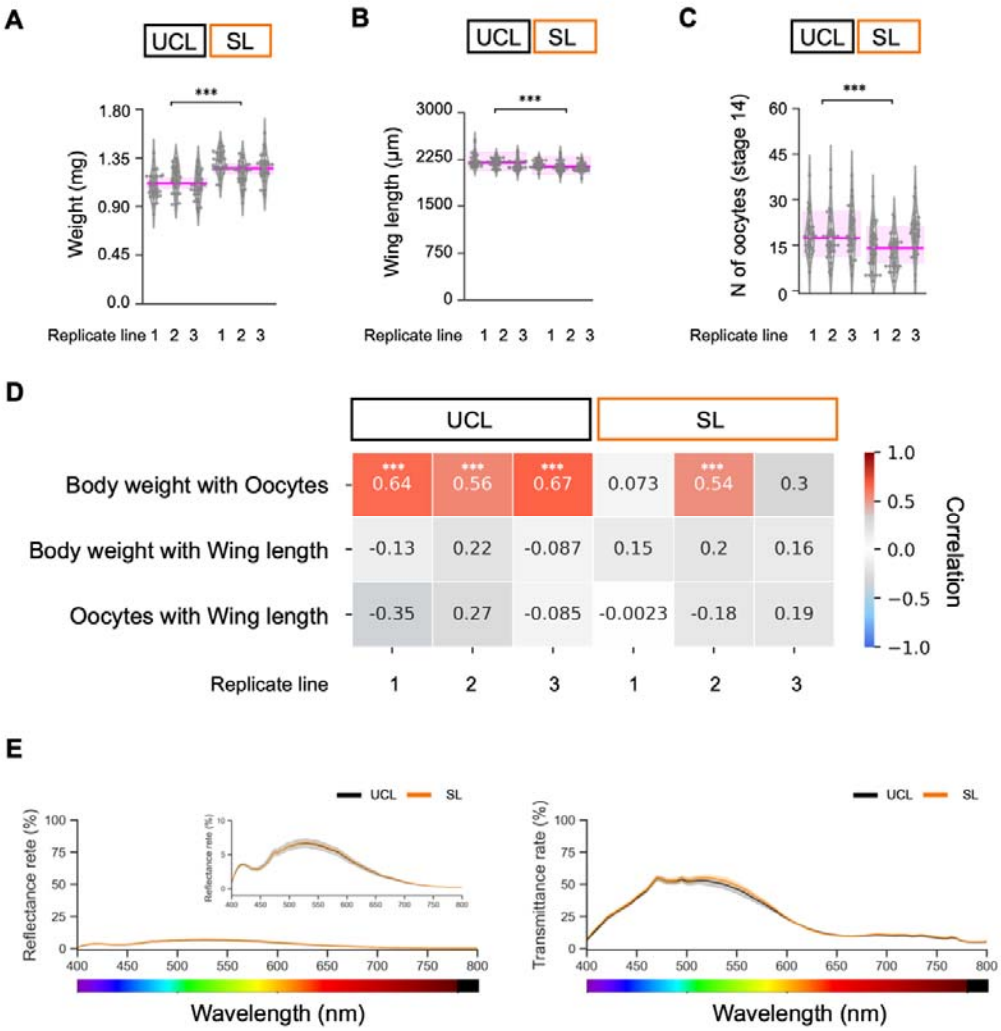

Figure. S2 | SL flies have heavier bodies, shorter wings, and fewer oocytes, but show no differences in light reflectance or transmittance.

A, Body weight. n = 90, BF_{10} > 100; generation 28. **B**, Wing length. n = 90, BF_{10} = 91.1; generation 28. **C**, Number of stage 14 oocytes. n = 90, BF_{10} = 2.46; generation 28. **D,** Correlation between traits, based on data from panels **A**–**C**. Asterisks indicate significance: *** p < 0.001. **E**, Reflectance rate and transmittance rate in female abdomens, n = 16; replicate line 1, generation 49. Statistical analyses for panels **A**–**C** were performed using a HBM with MCMC methods, posterior median, and Bayesian 95% CI. Asterisks indicate significance levels: *** pMCMC < 0.001. See Data S2 for details of all results, including statistical models.

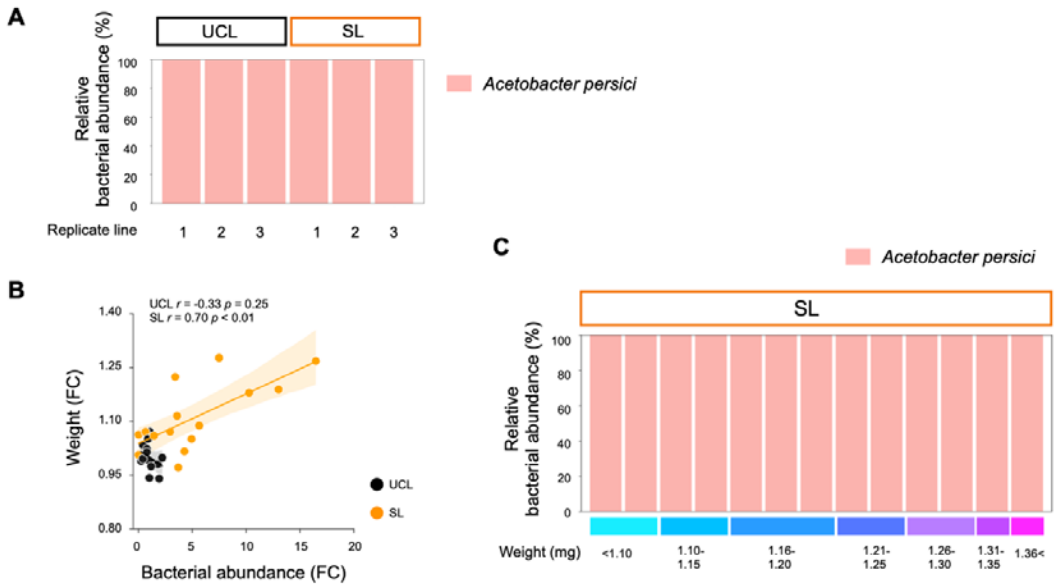

Figure. S3 | The gut microbiota of SL flies consists of a single *Acetobacter* species, with bacterial abundance positively correlated with body weight.

A, Relative bacterial abundance based on 16S/ITS rRNA amplicon sequencing in SL and UCL. The DNA samples used were the same as those used for whole-genome resequencing in Figure. 4a (generation 44). **B**, Correlation between body weight and bacterial abundance, based on data shown in Figure. 4A. The data were normalized to the mean UCL values from corresponding replicate lines. **c**, Relative bacterial abundance based on 16S/ITS rRNA amplicon sequencing in SL replicate line 1, generation 45. For details, see Data S3.

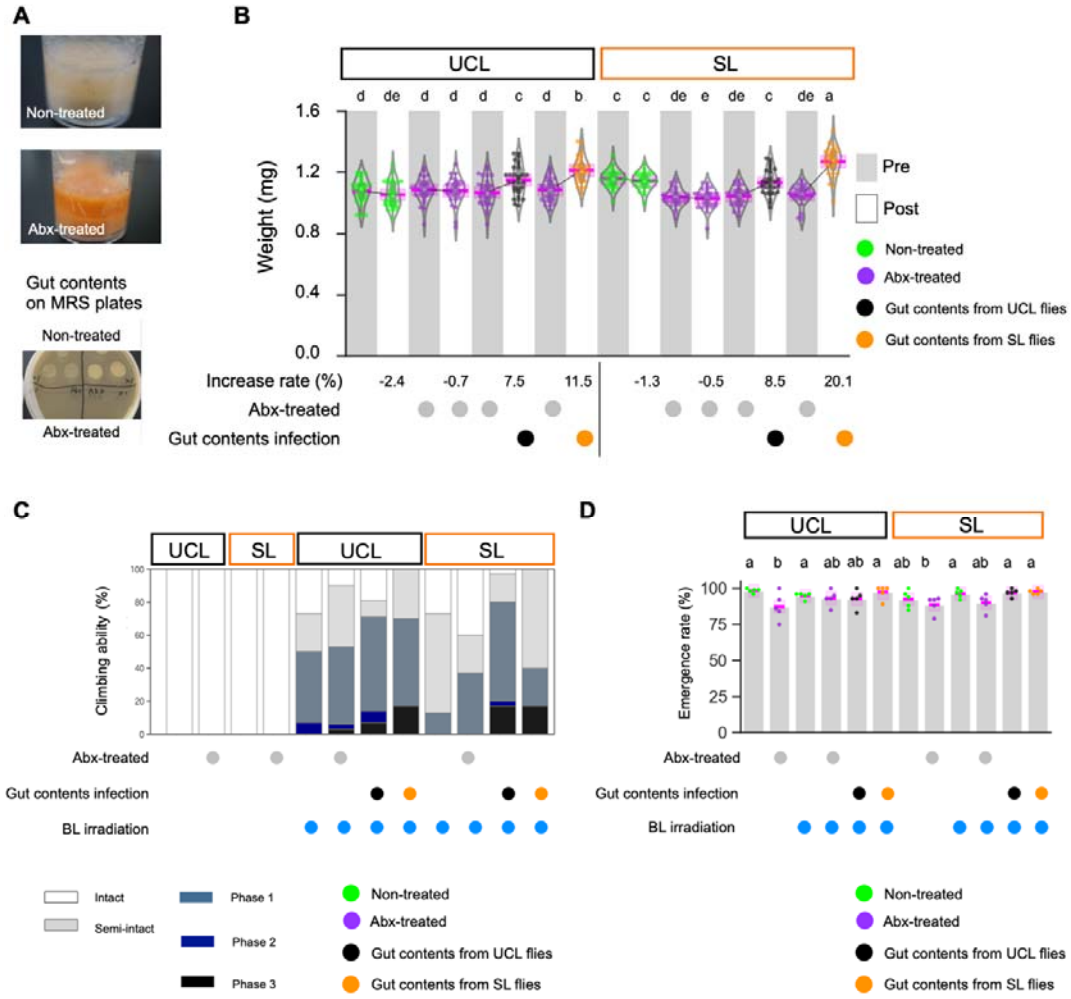

Figure. S4 | The unique phenotypes of SL flies depend on gut microbiota.

A, Effect of antibiotic mixture (Abx) treatment on gut microbiota. **B**, Impact of Abx treatment and infection with gut contents on body weight. Grey bars represent pre-infection, while white bars indicate post-infection after 4 days. n = 30, BF_{10} > 100; replicate line 1, generation 47. **C**, Climbing ability following BL irradiation. Each bar represents a total of 30 flies; replicate line 1, generation 47. **D**, Emergence rate, based on data shown in Figure. 3d. BF_{10} = 1.30; replicate line 1, generation 47.

Statistical analyses for panels **B** and **D** were performed using HBM with MCMC methods. Different letters indicate significant differences at pMCMC < 0.05. See Data S4 for details of all results, including statistical models.

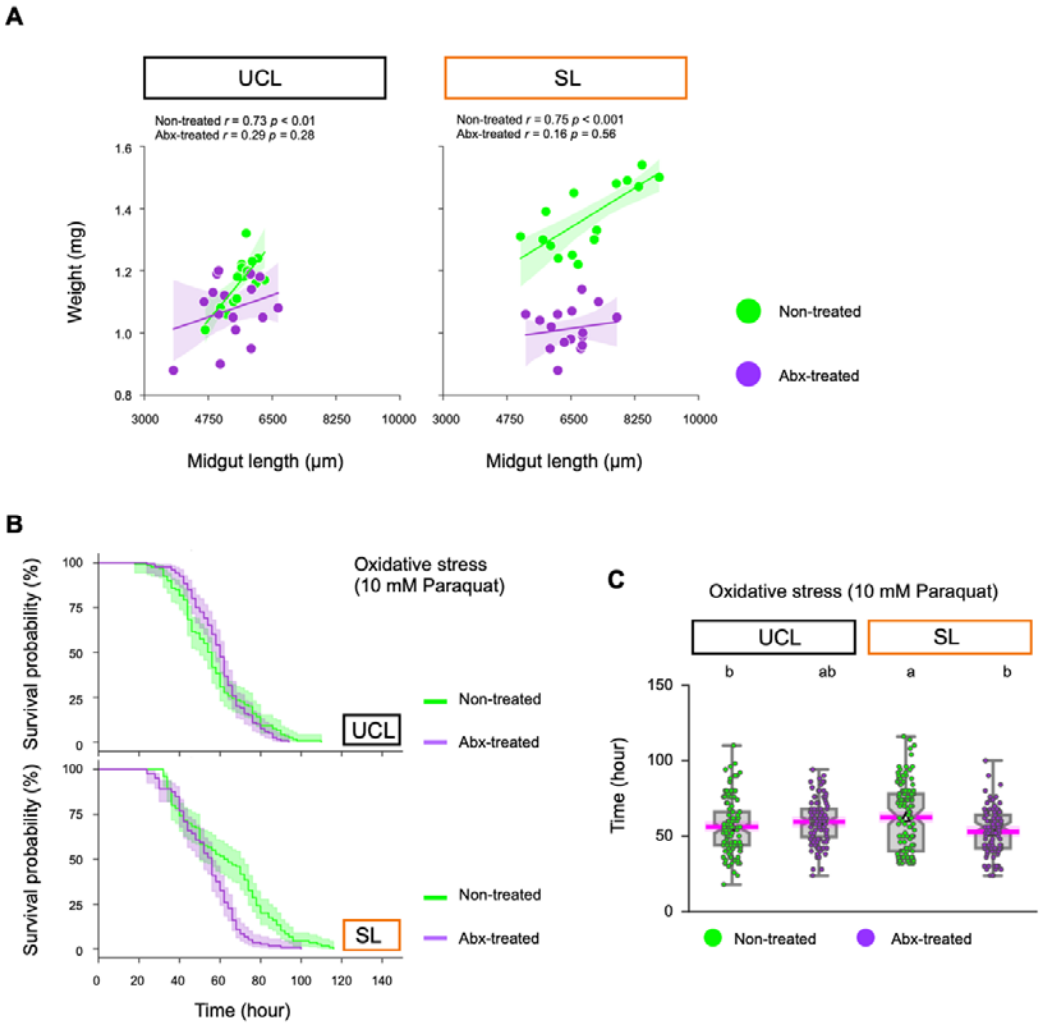

Figure. S5 | Gut microbiota-dependent physiological changes in SL flies

A, Correlation between body weight and midgut length, based on data from Figure. 4G. **B**, Oxidative stress resistance in SL flies treated with 10 mM paraquat. Kaplan–Meier survival curve, *n* = 120; replicate line 1, generation 52. **C**, Oxidative stress resistance in SL and UCL flies treated with 10 mM paraquat. *n* = 120, BF_{10} = 0.01. Survival: non-treated UCL 56.36 h (53.29–59.43), Abx-treated UCL 59.57 h (56.33–62.61), non-treated SL 62.48 h (59.42–65.64), Abx-treated SL 53.10 h (50.02–56.22); replicate line 1, generation 52.

Statistical analysis was performed using HBM with MCMC methods. Different letters indicate significant differences at *p*MCMC < 0.05. See Data S5 for details of all results, including statistical models.

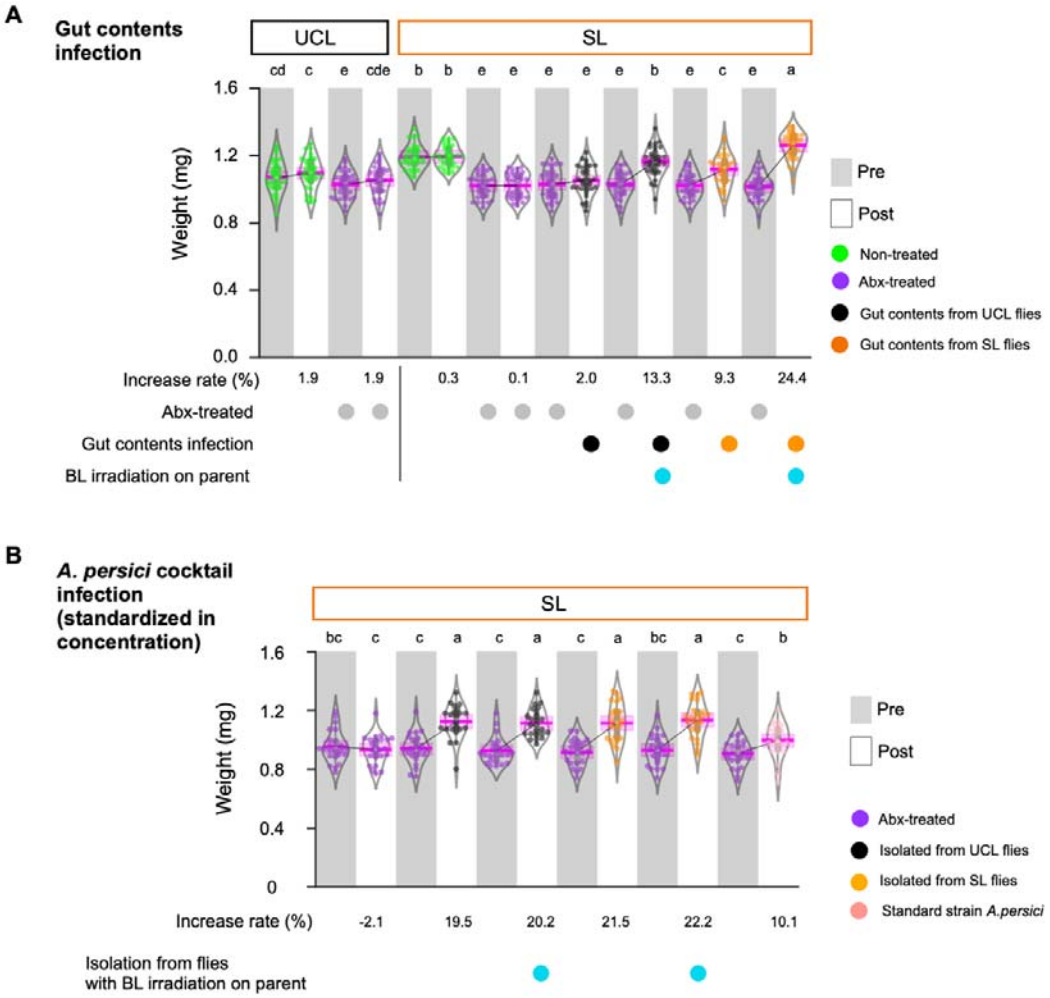

Figure. S6 | Greater bacterial abundance leads to higher body weight.

A, Impact of infection with gut contents on body weight. **B**, Impact of infection with *Acetobacter persici* cocktail on body weight. In both panels, grey bars represent pre-infection; white bars indicate post-infection after 4 days. n = 30, BF_{10} >100; replicate line 1, generation 53. Statistical analyses were performed using HBM with MCMC methods. Different letters indicate significant differences at pMCMC < 0.05. See Data S8 for details of all results, including statistical models.

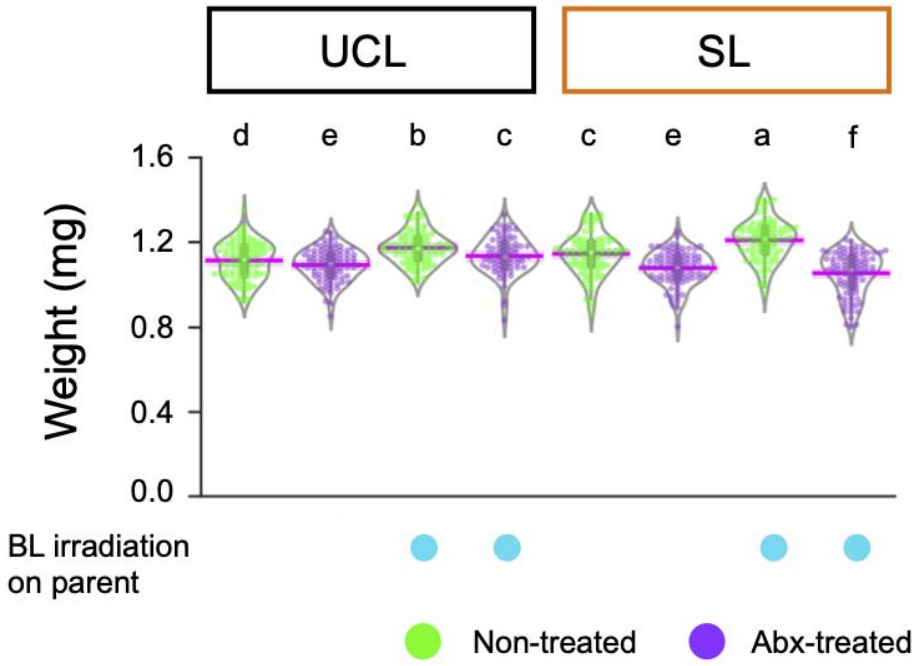

Figure. S7 | Parental BL experience increases body weight in progeny.

Data is based on female body weight. n = 72–90, BF_{10} > 100; replicate line 1, generation 46. Statistical analysis was performed using HBM with MCMC methods. Different letters indicate significant differences at pMCMC < 0.05. See Data S10 for details of all results, including statistical models.